UNIVERSITY OF WARMIA AND MAZURY IN OLSZTYN

Technical Sciences

16(3) 2013

PUBLISHER UWM

OLSZTYN 2013

The Technical Sciences is indexed and abstracted in BazTech (http://baztech.icm.edu.pl) and in IC Journal Master List (http://journals.indexcopernicus.com)

The Journal is also available in electronic form on the web sites
http://www.uwm.edu.pl/techsci (subpage Issues)
http://wydawnictwo.uwm.edu.pl (subpage Czytelnia)

The print edition is the primary version of the Journal

PL ISSN 1505-4675

Address
ul. Jana Heweliusza 14
10-718 Olsztyn-Kortowo, Poland
tel.: +48 89 523 36 61
fax: +48 89 523 34 38
e-mail: wydawca@uwm.edu.pl

Ark. wyd. 6,7, ark. druk. 5,5, nakład 120 egz.
Druk – Zakład Poligraficzny UWM w Olsztynie
zam. nr 616

Contents

Technical Sciences 16(3), 2013, 169–177

RELATIONSHIPS BETWEEN CFD AND EXPERIMENTAL FLUID MECHANICS

Wojciech Sobieski

Department of Mechanics and Machine Design
University of Warmia and Mazury in Olsztyn

Received 28 February 2013; accepted 26 August 2013; available on line 2 September 2013

K e y w o r d s: CFD, modeling methodology.

A b s t r a c t

This paper analyzes three popular methods of developing simulation models based on experimental data. The presented variants are discussed with emphasis on their strengths and weaknesses, and they are illustrated with examples in the area of numerical fluid mechanics. The principles of developing computer models, details and objectives of mathematical models are not discussed. The relevant information can be found in the author's previous studies which are available in scientific literature. The last section of the article proposes the most effective methods for combining and designing real and virtual experiments.

Introduction

Contemporary research in fluid mechanics relies mainly on three types of scientific activity: experiments, analyses and simulations. This division reflects the vastness of our knowledge resources and the need to select specific areas of expertise. The three types of activity can be integrated, but the results of such research often do not conform to the highest quality standards, and a greater degree of specialization may be required. When research projects are conducted in a single field of inquiry, specialization brings significant benefits and it is highly effective. Despite the above, there is a growing demand for interdisciplinary projects which combine knowledge not only from different branches of the same science, but also from very distant areas of study. The above calls for the development of a global research strategy that would make the best use of

* Corespondence: Wojciech Sobieski, Katedra Mechaniki i Podstaw Konstrukcji Maszyn, Uniwersytet Warmińsko-Mazurski, ul. M. Oczapowskiego 11, 10-957 Olsztyn, phone: +48 89 523 32 40, e-mail: wojciech.sobieski@uwm.edu.pl.

human potential. This concept is discussed in the first part of the article. The second part of this paper describes three examples of projects based on different research concepts, and it highlights the problems arising from their performance. This paper was motivated by the author's experiences and observations made during various research projects performed individually and in collaboration with other researchers and teams. This article highlights the main problems which result from the integration of experiments, analyses and simulations in the area of fluid mechanics, and it proposes practical solutions for overcoming those difficulties. It has been assumed that an experiment is the most important stage of research and that a virtual model has to be based on experimental data. This assumption follows from the general principle that a simulation model is of value when it conforms to real world observations.

Integrated fluid mechanics models

The first method of integrating experimental studies with numerical analyses in fluid mechanics is illustrated in Figure 1*a*. It begins with an experiment whose results are used to develop a simulation model. In this variant, information flows in one direction only: from the experiment to the simulation model. The above is observed in two cases. In the first case, a virtual model is developed based on an experiment described in literature. The developer of a simulation model is generally unable to acquire additional data and has to rely on the information available in published articles. If the experiment is well described, additional calculations can be performed to obtain new data. Analytical mechanics can act as a bridge between the experiment and the numerical model. In the second case, a simulation model is developed based on an experiment which was conducted by one researcher, a team or a different research group, preferably one that which can be directly contacted. It is assumed that the experiment cannot be wholly replicated for some reason (such as cost). Nevertheless, this case is more conducive to research than the first scenario because experimental data can be verified despite the lapse of time. The researcher can validate information relating to instruments, measurement methods, measurement accuracy, flow geometry and parameters of flow media used in the study. In some cases, additional experiments can be performed.

In the second variant (Fig. 1*b*), a previous experiment, which was not initially planned as a source of data for numerical modeling, can be replicated. In this approach, a virtual model is first developed based on measurements, the results of calculations (preferably subjected to a sensitivity analysis) are

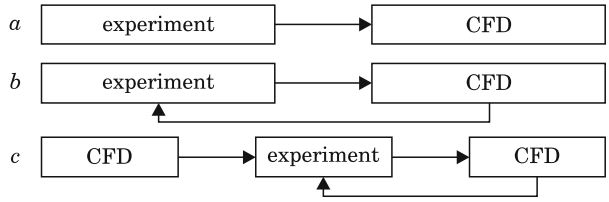

Fig. 1. Basic approaches to integrating experiments in fluid mechanics with CFD

analyzed, and the experiment is replicated in view of the specific needs of the numerical model. Changes in measurement methods or instruments could be required due to a need for new data or the imprecision of measurement results. Those treatments could increase the degree of cohesion between an experiment and a virtual model, improve the compatibility and quality of results produced by both types of activity. A satisfactory degree of result cohesion testifies to the quality of the numerical model and the experiment. This issue was discussed in greater detail by SOBIESKI (2009 and 2010).

In the third variant (Fig. 1*c*), the project begins with the development of a preliminary simulation model based on data estimation. General principles for developing a successful computer model are reviewed at this stage. Sets of "closures", i.e. fragments of a global mathematical model describing specific problems, which are used by other authors should be collected and analyzed. A sensitivity analysis is also recommended at this stage. In the analysis, the modeled parameters are changed (preferably by a constant value, e.g. $\pm 5 \div 10$), and the impact of those changes on the results is observed. This problem has been discussed earlier, for example by SOBIESKI (2008b, 2008d). If the resulting changes are significant, the model is sensitive to the analyzed parameter, whereas minor changes indicate that the model is characterized by low sensitivity. A sensitivity analysis can be performed in most cases, not only when a numerical approach (CFD) is adopted. It supports the identification of parameters which should be of the highest quality. The resulting knowledge can be used in designing the experiment, selecting measuring methods and the precision of instruments. The correct performance of this stage will increase the reliability of the simulation model, and it will minimize the probability that errors resulting from low quality data surface in successive stages of research. Detailed knowledge about the possibilities and needs of the simulation model is required for designing the experiment. Additional simulations and a virtual evaluation of the future test stand can be performed at the planning stage. After the experiment has been performed and the required data has been collected, simulations can be repeated, this time with the use of real rather than estimated data. Further course of action will be determined by the degree of cohesion between the virtual model and the

experiment. If the degree of cohesion is unsatisfactory, the simulation model and/or the experiment can be reevaluated, corrections can be introduced and the entire cycle can be repeated.

The discussed variants of integrating experiments and numerical analyses in fluid mechanics apply to situations which are most frequently encountered in practice. In large and complex projects, other scenarios are also possible (e.g. experimental and numerical analyses can be conducted simultaneously by two collaborating teams, simulation models can be developed for new and unresolved research problems or experiments can be planned for theoretically predicted phenomena), but they are relatively rare, and they will not be discussed in this article. Although many tips and suggestions described in this paper may seem to be obvious, the authors' observations indicate that the simplest and the most obvious principles are often disregarded in practice. The aim of this paper is to encourage scientists to thoroughly analyze research procedures at early stages of the project. The resulting knowledge will significantly facilitate the integration of experiments and virtual models at successive phases of research.

An example of variant *A* – bifurcation modeling in a closed-off channel

Bifurcation modeling in a closed-off channel can serve as an example of a simulation model based on an experiment described in literature. The source of data was a study by DYBAN et al. (1971) which discusses a series of 2D experiments where fluid (air or water) was pumped through a nozzle to a closed-off channel with varied geometry (the variable parameters were nozzle width and channel length). Flow structures formed inside the channel were observed. In the analyzed system, the created structures were determined mainly by channel and nozzle geometry, defined as b/B and H/B, where b is nozzle width, B – channel width and H – channel length measured from the end of the supply nozzle. Other factors, such as the type of medium and its parameters, were of secondary importance, and they merely shifted the range at which different types of bifurcations appeared. The flow structures identified in the simulation model were identical to those noted in the experiment, and a structure not described by the authors was additionally observed. The results of the experiment are discussed in depth by SOBIESKI (2008d). Older results can be found in SOBIESKI (2008a). In the cited study, only a high degree of qualitative cohesion was noted (Fig. 2). The degree of quantitative cohesion was not determined due to a shortage of relevant data in the source article. The lack of data caused by one-directional flow of information is the main constraint in the discussed variant.

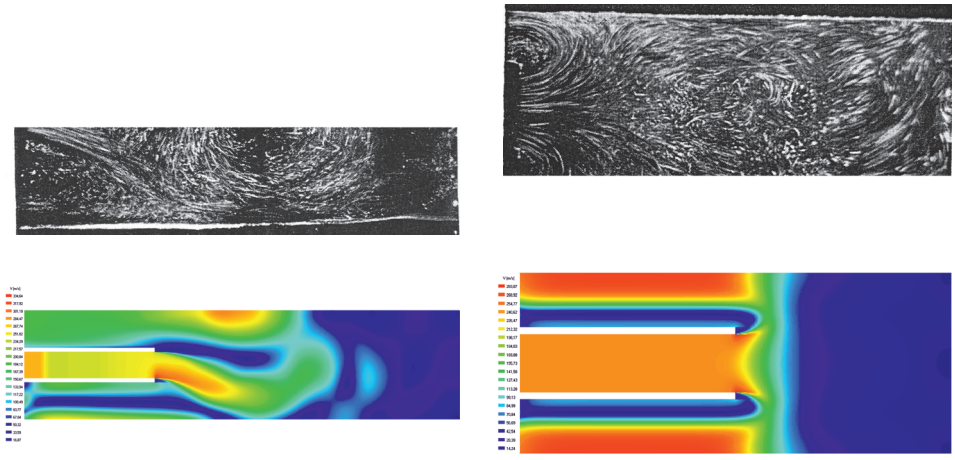

Fig. 2. Qualitative comparison of experimental and simulation results:examples of oscillating (left) and divergent bifurcations (right)

An example of variant *B* – fluid dynamics modeling in a spouted-bed grain dryer

This example discusses the process of modeling fluid dynamics in a spouted-bed grain dryer which was performed by an independent research team collaborating with the author. In the first stage, a simulation model was developed based on an existing set of measurement data. The results of numerical calculations were highly unsatisfactory, and studies reporting a much higher degree of cohesion between experimental data and simulation results were available in literature, for example in the work of SZAFRAN (2004). Initially, attempts were made to identify the causes of the above discrepancies by analyzing the configuration of the simulation model and the selection of "closures", but the quality of the experiment was not investigated. Those efforts did not bring satisfactory results (but a significant improvement in results was achieved when the concept of a sphericity coefficient was introduced into the mathematical model), and a sensitivity analysis was performed to test the model's responses to changes in the modeled parameters. The results are discussed by SOBIESKI (2008b, 2008c) and SOBIESKI, MARKOWSKI (2006).

The sensitivity analysis proved to be a key step to solving the problem. It revealed that the simulation model was most sensitive to the airflow rate at dryer inlet, equivalent grain diameter and maximum bed packing. Those parameters, in particular the method and precision of their determination, were thoroughly analyzed. The method of determining airflow rate was found to be highly inaccurate (for more information, refer to SOBIESKI 2009f). In the

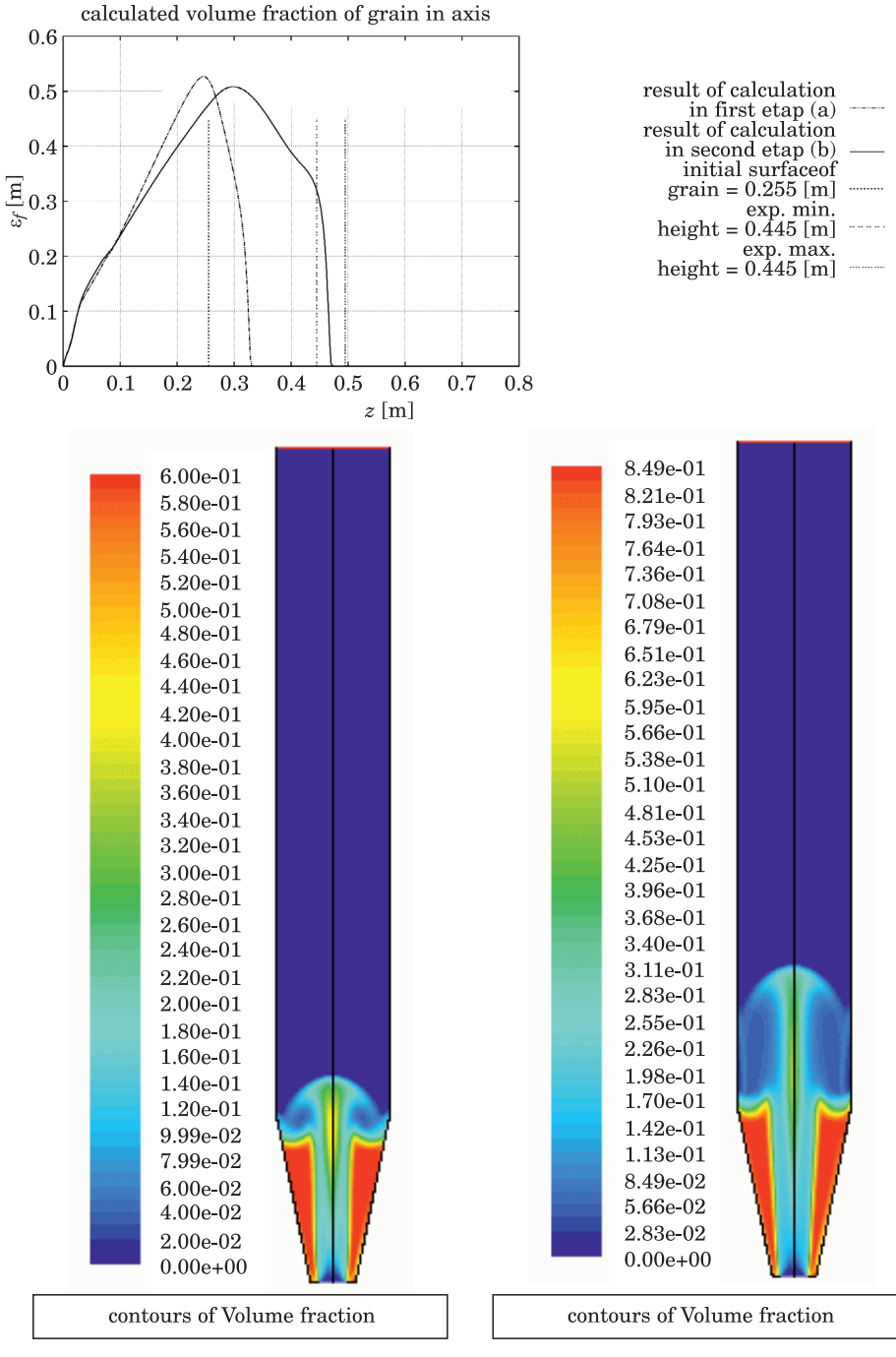

Fig. 3. Comparison of experimental and numerical results in the initial and final stages of the study

experiment, an anemometer was installed at the outlet of the dryer column in a manner that caused significant leakage. The device was equipped with a Pitot tube, but it was not used in most cases. According to experiment notes, airflow rate measured by an alternative method was more than 10% higher than that determined initially. When new data was input into the numerical model, the results were highly satisfactory. The results of both simulation phases are compared in Figure 3.

The experiment was repeated based on the new knowledge about conditions that guarantee cohesion between experimental and modeled results. This time, the general parameters were somewhat modified by the new context, but the accumulated experiences facilitated the development of a satisfactory simulation model. All parameters had to be repeatedly determined, in particular equivalent grain diameter and maximum degree of packing. Simulation results and selected aspects of fluid dynamics modeling in spouted-bed grain dryers were discussed in a series of publications by SOBIESKI (2008d, 2009a, 2009e, 2010a, 2011) and in the work of SOBIESKI (2008e, 2009d). The main weakness of the analyzed variant is that the experiment has to be partially repeated, which is a waste of resources and time. If all parameters were measured with the required accuracy and in the required manner from the beginning of the experiment, the cohesion between experimental and modeled results would have been achieved much earlier. Sound knowledge of numerical modeling conditions is of essence, and teams which possess such knowledge can perform experiments which constitute a reliable basis for developing simulation models.

An example of variant *C* – modeling flow resistance in porous media

The third example discusses the modeling of flow resistance in porous media based on an experiment which was performed by the author during a research placement at the University of Manitoba in Winnipeg, Canada. Similar research had been previously carried out by the author in Poland, but at that time, variant *B* had to be deployed due equipment constraints. In the new study, the test stand had to be built from scratch. New research objectives were also formulated: to analyze the bed's lay pattern and to measure and model flow resistance in two spatial directions. Several test stands were proposed and analyzed. Two of them were modeled with the use of CFD methods. The selected variant was built by the technical group. The final simulation model, where only several experimental parameters had to be input, and supporting software were developed. Measurements were per-

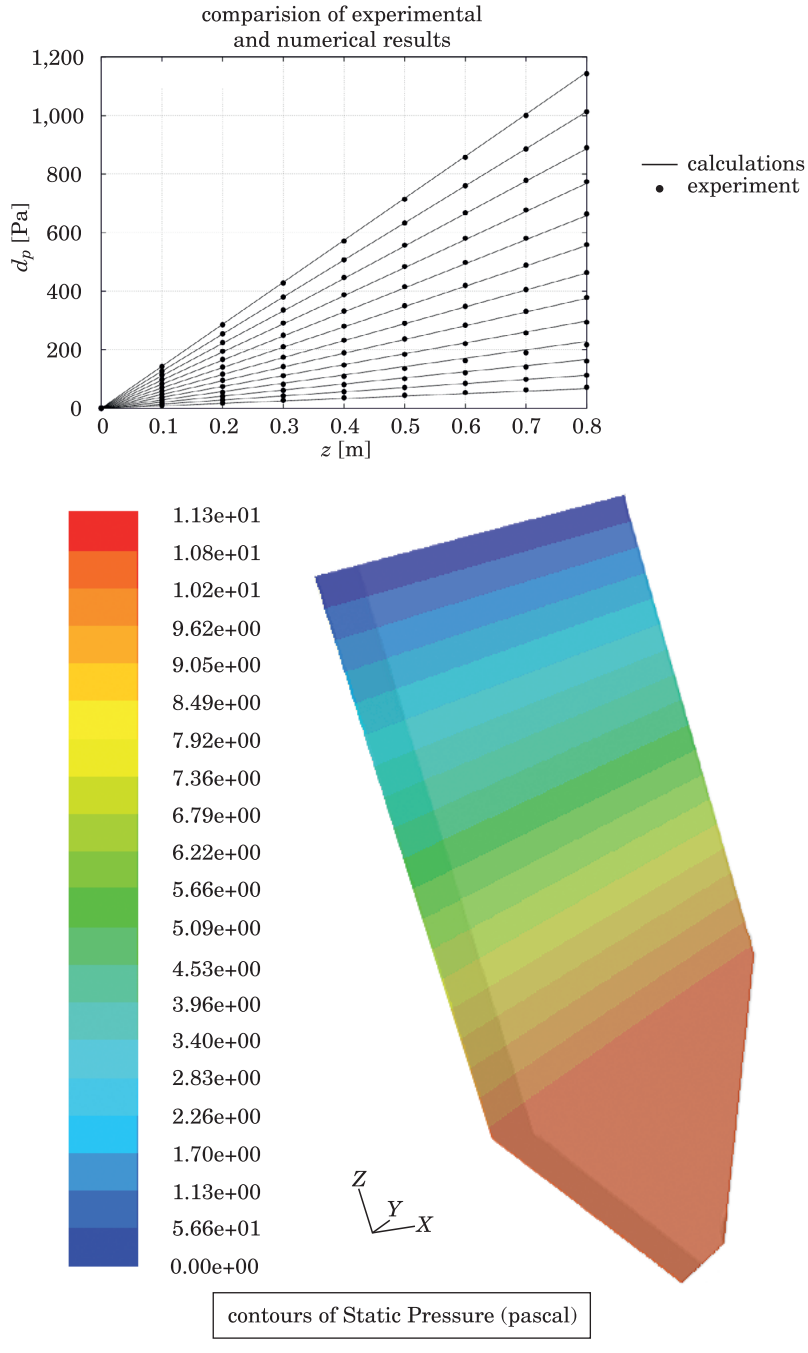

Fig. 4. Comparison of experimental and numerical results: decrease in pressure at various airflow rates (left); visualization of pressure distribution in the bed (right)

formed and the results were processed. Qualitative and quantitative cohesion between experimental and modeled data was achieved within several hours. The project's success resulted from careful preparations which involved analyses of all possible relations between the experiment and the simulation model.

Conclusions

The following conclusions can be formulated based on the discussed topics:

– In general, experiments described in literature should be used only for learning how to model certain phenomena and for developing estimation models. The knowledge of modeling principles is very important because flow problems, in particular multiphase flows, are highly complex (both mathematically and technically), and high quality literature may be difficult to find. Learning about a new problem is a long process that involves reading CFD software documents, analyzing articles, courses and examples, browsing internet resources and consulting members of the scientific community. The learning process is complete when mathematical modeling problems have been solved and an operating and stable model has been built.

– When modeling efforts are based on an experiment described in literature, researchers could benefit from exchanging experiences and data with the experiment's authors. If collaboration is not possible, other experiments could be considered – effective communication with the authors increases the chances of the project's success.

– Experiments described in literature should constitute a theoretical basis in the initial stages of follow-up research. Literature should be reviewed for a better insight into the current state of research in a given area, the identified problems and attempts to solve them. The first estimation model can be developed based on the acquired knowledge. The model can be used to repeat a previous experiment (variant *B*) or design a new one (variant *C*).

– Research conducted in variant *B* is a natural consequence of experimental studies. The experimental approach may become somewhat "uninspiring" when most aspects of a given problem have been measured and described. Numerical analysis encourages further scientific inquiry, and it motivates researchers to tackle new challenges. Numerical analyses and experiments can be performed by the same person or by different people as long as they collaborate in their efforts.

– Variant *C* is preferred when new research projects are initiated and when new equipment has to be purchased or designed and built. A preliminary numerical model can be used to adapt purchase and design decisions to the

needs of a simulation model. This approach will minimize experimental costs, and it will shorten the time during which cohesion is achieved between experimental and numerical results.

Regardless of the adopted method of integrating experiments and numerical models, researchers should have sound knowledge of their possibilities and limitations. This is particularly important when experiments and numerical analyses are performed by different persons or teams. Potential problems should be identified and solved in early stages of research to prevent unnecessary project costs and delays.

References

BADUR J., SOBIESKI W. 2001. *Numerical simulation of Hopf bifurcations in a turning off flow*. Research of the Chair of Mechanics and Machine Design, p. 63–98, Olsztyn.

DYBAN E.P., MAZUR A.I., JEPIK J.J. 1971. *Osobennosti istechenija plaskoj vojedushhnoj strui v tupik*. Teplofizika i Teplomehanika, 19: 41–45.

SOBIESKI W. 2007. *Numerical Modeling of Fluidised Beds with the Use of the Eulerian Multiphase Model*. Professor Zbigniew Bilicki in Memoriam – Symposium. Gdańsk–Wieżyca, June 18–20.

SOBIESKI W. 2008a. *Basic Principles and Stages of Computer Modeling in Fluid Mechanics*. In: *Elements of agricultural system engineering*. University of Life Sciences, Poznań, pp. 111–129.

SOBIESKI W. 2008b. *Indicator of Fluidized Bed Computer Model Sensitivity to Changes in Physical Parameters' Values*. Annual Review Of Agricultural Engineering, 6(1): 51–58.

SOBIESKI W. 2008c. *Influence of Selected Eulerian Multiphase Model Parameters on the Simulation Results for a Spouted Bed Grain Dryer*. Task Quarterly, 12(1): 511–536.

SOBIESKI W. 2008d. *Numerical Analysis of Sensitivity of Eulerian Multiphase Model for a Spouted Bed Grain Dryer*. Drying Technology, 26(12): 1438–1456.

SOBIESKI W. 2008e. *Numerical Modeling of Spouted Fluidised Beds*. IV International Congress of Technical Diagnostics. Olsztyn, September 9–12.

SOBIESKI W. 2009a. *Momentum Exchange in Solid-Fluid System Modeling with the Eulerian Multiphase Model*. Drying Technology, 27(5): 653–671.

SOBIESKI W. 2009b. *Numerical Analysis of Flow Bifurcations in a Closed-Off Channel*. Technical Sciences, 12: 272–285.

SOBIESKI W. 2009c. *Numerical and Experimental Analyses of Hopf Bifurcations in a Locally Expanded Channel*. Technical Sciences, 12: 259–271.

SOBIESKI W. 2009d. *Selected Problems of Numerical Modeling of Fluidized Bed in a Spouted Grain Dryer*. Chemical Engineering and Apparatus, 1: 68–69.

SOBIESKI W. 2009e. *Switch Function and Sphericity Coefficient in the Gidaspow Drag Model for Modeling Solid-Fluid Systems*. Drying Technology, 27(2): 267–280.

SOBIESKI W. 2009f. *Use of Simulation Methods to Validate the Results of an Experiment*. In: *Knowledge Engineering and Expert Systems*. EXIT Publisher, Warsaw, pp. 113–124.

SOBIESKI W. 2010a. *Selected Aspects of Developing a Simulation Model of a Spouted Bed Grain Dryer Based on the Eulerian Multiphase Model*. Drying Technology, 28(12): 1331–1343.

SOBIESKI W. 2010b. *Use of Numerical Models in Validating Experimental Results*. Journal of Applied Computer Science, 18(1): 49–60.

SOBIESKI W. 2011. *Drag Coefficient in Solid-Fluid System Modeling with the Eulerian Multiphase Model*. Drying Technology, 29(1), pp. 111–125.

SOBIESKI W., MARKOWSKI M. 2006. *The Investigations of Fluid Dynamics and Mass Transfer in a Spouted Dryer*. The 6th Workshop of "Modeling the Multiphase Flows in Thermo-Chemical Systems – Numerical Methods". Stawiska, September 4–6.

SZAFRAN R. 2004. *Modeling of Drying in a Spouted Bed Dryer*. Ph.D. Thesis., Wrocław.

Technical Sciences 16(3), 2013, 179–192

EXAMPLE OF ROBUST FREE ADJUSTMENT OF HORIZONTAL NETWORK COVERING DETECTION OF OUTLYING POINTS

Marek Hubert Zienkiewicz, Tomasz Bałuta

Institute of Geodesy
University of Warmia and Mazury in Olsztyn

Received 27 November 2012; accepted 31 July 2013; avilable on line 2 August 2013

K e y w o r d s: free adjustment, robust estimation.

A b s t r a c t

This paper presents the method of detecting outlying reference points by applying robust free adjustment. The article contains the theoretical basis of the robust free adjustment. Theoretical considerations are supplemented by a numerical example showing the possible practical applications. In this paper is also included example, which presents detecting of reference points contaminated by gross error, in the case of existence gross errors in observation sets.

Introduction

Theory of the robust adjustment of observation set is one of the most rapidly developing estimation methods. Development of methods of the geodetic networks adjustment concern, especially the robust adjustment for gross errors. General idea of the robust estimation is identify and reduce influence of outliers in the adjustment solution. Reduce the influence of the outliers or their complete elimination can be achieved by damping weights of observations (e.g. HUBER 1981, YANG 1994). It is a very useful property, especially in the analysis of deformation. In the measurements of displacement and deformations, gross errors, may occur not only in the observation but also, in the coordinates of reference points. This may be related to the situation

Corespondence: Marek Zienkiewicz, Instytut Geodezji, Uniwersytet Warmińsko-Mazurski, ul. Oczapowskiego 1, 10-719 Olsztyn, phone: +48 89 523 60 25, e-mail: marek.zienkiewicz@uwm.edu.pl

when the reference point is displaced. It is obvious that performing the correct interpretation of the results is dependent of the reference points. There are known a lot of robust methods concerned a control of reference mark stability (e.g. DUCHNOWSKI 2010). In practice, there might be also other situations, that are related with the change of the reference points coordinates. It happens when the coordinates of the point are contaminated by gross errors due to incorrectly inputted data. It is known that if we take that point as a fixed point during adjustment, then the results of the adjustment will be incorrect. In such cases detection of the contaminated point of the network can be obtain by the robust free adjustment. The identification of the contaminated points and reduction of their influence on the final result of the adjustment was proposed in (WIŚNIEWSKI 2002). Making the geodetic network "free" and applying the robust free adjustment, large increments to the outlying coordinate can be expected. Reduce influence of the contaminated coordinates on the final adjustment results can be obtain by modifying elements of the coordinates weight matrix. Simultaneously are designated the values of outlying coordinates. The principles of the robust free adjustment are related to the classical method of the robust M – estimation (WIŚNIEWSKI 2005). In practice, there might be a situation where besides gross errors in the coordinates, a gross errors in the observations may also occur. In such case it is recommend to apply the hybrid M – estimation (CZAPLEWSKI 2004). In this method occurs both, damping weights of the coordinates weight matrix and damping weights of the observations weight matrix.

Theoretical foundation of free adjustment of the geodetic network

The classical estimation methods assume, that the coefficients matrix $\mathbf{A}$ is a column, full rank matrix (WIŚNIEWSKI 2005). Then the matrix $\mathbf{A}^T\mathbf{PA}$ (where $\mathbf{P}$ is weight matrix of observations) is a non-singular matrix, and its inverse is following $(\mathbf{A}^T\mathbf{PA})^{-1}$. In case of the free geodetic network, rank of the matrix $\underset{n,m}{\mathbf{A}}$ (where n is the number of observations and m is the number of the parameters) is less then quantity of its columns and difference between both values is equal to the defect (further: d) of matrices, i.e. $d = m - \text{ranki}(\mathbf{A})$. In case of geodetic networks defect of matrices $\mathbf{A}$, can be identified with the freedom degrees relative to the adopted coordinate system (external degrees of freedom). A properly chosen network cannot have internal degrees of freedom (e.g. similarity). Thus, angular – linear network (2D network) has three degrees of freedom (further: SW) – displacement due to X, Y axes and rotation. Assume that at the network shown in Figure 1 the points 1^o, 2^o, 3^o have the

approximate coordinates, and the points $\hat{1}$, $\hat{2}$, $\hat{3}$, have estimated coordinates. Due to the fact, that network is free ($SW = 3$), all of the adjustment points may be displaced relative to the approximate points. The main aim of the free adjustment is optimal fitting adjustment network to approximate network.

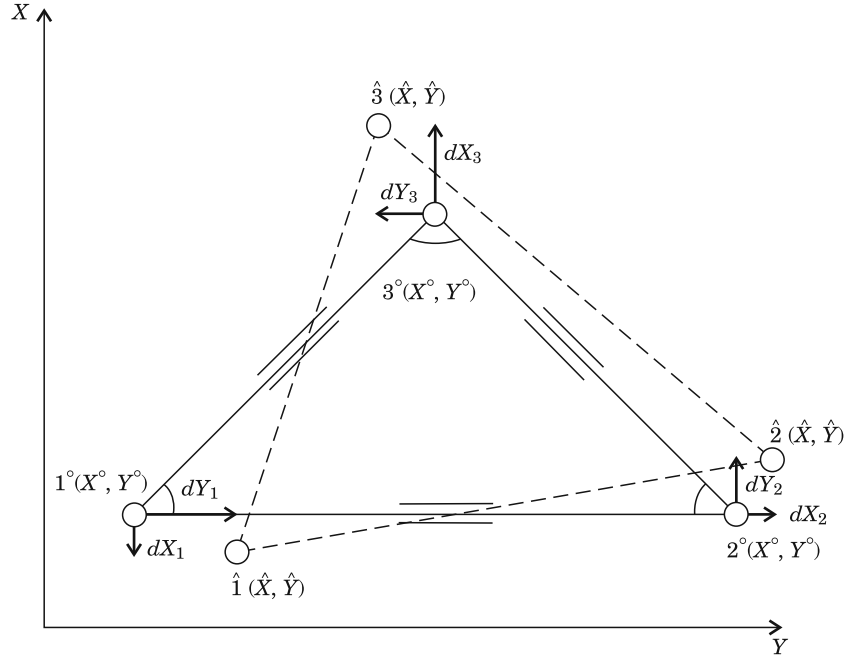

Fig. 1. Geometric interpretation of the free adjustment

Under consideration in the free adjustment of geodetic networks, where defect is different from zero, should be additional criterion for increments dX_i, dY_i for all points in the network. Provided that criterion has a form $\Phi_X(d\mathbf{X}) = d\mathbf{X}^T\mathbf{P}_\mathbf{X}d\mathbf{X} = \min.$,solution of the free adjustment problem can be represented by the following equations (WIŚNIEWSKI 2005).

$$\begin{cases} \mathbf{V} = \mathbf{A}d\mathbf{X} + \mathbf{L} \\ \Phi(d\mathbf{X}) = \mathbf{V}^T\mathbf{P}\mathbf{V} = \min. \\ \Phi_X(d\mathbf{X}) = d\mathbf{X}^T\mathbf{P}_\mathbf{X}d\mathbf{X} = \min. \end{cases} \tag{1}$$

where $\mathbf{P}_\mathbf{X}$ is matrix of parameters weights $\mathbf{X}$, and thus the weights matrix of demanding increments $d\mathbf{X}$. Solving this problem it is necessary to take into account only the aim function $\Phi(d\mathbf{X}) = \mathbf{V}^T\mathbf{P}\mathbf{V}$ which gives normal equations

$\mathbf{A}^T\mathbf{PA}d\mathbf{X} + \mathbf{A}^T\mathbf{PL} = \mathbf{0}$ with a singular matrix of coefficients $\mathbf{A}^T\mathbf{PA}$. Having matrix $\mathbf{A}$ and vector $d\mathbf{X}$ in the following forms:

$$\underset{n,m}{\mathbf{A}} = \begin{bmatrix} \underset{n,r}{\mathbf{A}_r} & \underset{n,d}{\mathbf{A}_d} \end{bmatrix}, \; d\mathbf{X} = \begin{bmatrix} \underset{1,r}{d\mathbf{X}_r^T} & \underset{1,d}{d\mathbf{X}_d^T} \end{bmatrix},$$

where $r = \operatorname{rank}(\underset{\text{mxm}}{\mathbf{A}^T\mathbf{PA}})$, normal equations can be written in following way:

$$\mathbf{A}^T\mathbf{PA}d\mathbf{X} + \mathbf{A}^T\mathbf{PL} = \mathbf{0} \Leftrightarrow \tag{2}$$

$$\begin{bmatrix} \mathbf{A}_r^T \\ \mathbf{A}_d^T \end{bmatrix} \mathbf{P}[\mathbf{A}_r \; \mathbf{A}_d] \begin{bmatrix} d\mathbf{X}_r \\ d\mathbf{X}_d \end{bmatrix} + \begin{bmatrix} \mathbf{A}_r^T \\ \mathbf{A}_d^T \end{bmatrix} \mathbf{PL} = 0 \Leftrightarrow \tag{3}$$

$$\begin{bmatrix} \mathbf{A}_r^T\mathbf{PA}_r & \mathbf{A}_r^T\mathbf{PA}_d \\ \mathbf{A}_d^T\mathbf{PA}_r & \mathbf{A}_d^T\mathbf{PA}_d \end{bmatrix} \begin{bmatrix} d\mathbf{X}_r \\ d\mathbf{X}_d \end{bmatrix} + \begin{bmatrix} \mathbf{A}_r^T\mathbf{PL} \\ \mathbf{A}_d^T\mathbf{PL} \end{bmatrix} = 0 \tag{4}$$

In this way we get a system consisting of two matrix equations. They contain r and d of equations respectively. Due to the fact that the rank $(\underset{\text{mxm}}{\mathbf{A}^T\mathbf{PA}}) = r$, so this matrix is singular. So if the vector of increments $d\mathbf{X} = \begin{bmatrix} d\mathbf{X}_r \\ d\mathbf{X}_d \end{bmatrix}$ has solution of the first matrix system, then we can certainly say that it has also solution of the second matrix system. Therefore, a system of two matrix equations may be replaced by the first of them (SZUBRYCHT, WIŚNIEWSKI 2004, WOLF 1972).

$$\mathbf{A}^T\mathbf{PA}d\mathbf{X} + \mathbf{A}^T\mathbf{PL} = \mathbf{0} \Leftrightarrow$$

$$\mathbf{A}_r^T\mathbf{PA}_r d\mathbf{X}_r + \mathbf{A}_r^T\mathbf{PA}_d d\mathbf{X}_d + \mathbf{A}_r^T\mathbf{PL} = \mathbf{0} \tag{5}$$

with nonsingular matrix of coefficients $\mathbf{A}_r^T\mathbf{PA}_r$. This is consistent with the conception of minimum norm g – inverse (RAO 1973). The first system of normal equations consist of r independent equations with $m = r + d$ unknowns. Because of the datum defect exist, so this is a system of equation with more quantity of unknowns than equations. The quantity of equation in the second system of equations is equal to the defect of network. It means that equations forming second system of equations are independent from the equations of first system (SZUBRYCHT, WIŚNIEWSKI 2004). Therefore, the system (4) can be written in the form (5). Derivation matrix

$$\mathbf{B} = [\mathbf{A}_r^T\mathbf{PA}_r \;\; \mathbf{A}_r^T\mathbf{PA}_d] \tag{6}$$

equations (5) can also be written as

$$\mathbf{B}d\mathbf{X} + \mathbf{A}_r^T\mathbf{PL} = \mathbf{0} \tag{7}$$

After partial (only with function $\Phi(d\mathbf{X}) = \mathbf{V}^T\mathbf{PV} = \min.$) solving the task (1), the final optimization form is obtained

$$\begin{cases} \mathbf{B}d\mathbf{X} + \mathbf{A}_r^T\mathbf{PL} = \mathbf{0} \\ \Phi_X(d\mathbf{X}) = d\mathbf{X}^T\mathbf{P}_\mathbf{X}d\mathbf{X} = \min. \end{cases} \tag{8}$$

This is conditional equation and using Lagrange's functions can be replaced by formula

$$\begin{cases} \mathbf{B}d\mathbf{X} + \mathbf{A}_r^T\mathbf{PL} = \mathbf{0} \\ \Phi_{XL}(d\mathbf{X}) = \Phi_X(d\mathbf{X}) - 2\mathbf{K}^T(\mathbf{B}d\mathbf{X} + \mathbf{A}_r^T\mathbf{PL}) = \\ = d\mathbf{X}^T\mathbf{P}_\mathbf{X}d\mathbf{X} - 2\mathbf{K}^T(\mathbf{B}d\mathbf{X} + \mathbf{A}_r^T\mathbf{PL}) = \min. \end{cases} \tag{9}$$

where $\mathbf{K}$ is correlative vector (Lagrange's multipliers). The solution (9) is a vector (WIŚNIEWSKI 2005):

$$d\hat{\mathbf{X}} = -\mathbf{P}_\mathbf{X}^{-1}\mathbf{B}^T(\mathbf{B}\mathbf{P}_\mathbf{X}^{-1}\mathbf{B}^T)^{-1}\mathbf{A}_r^T\mathbf{PL} \tag{10}$$

Accuracy analysis of the free adjustment is similar to the classic adjustment. During calculation estimator of the variance coefficient, it should be taken into consideration that the number of redundant observation is increased by defect network. This estimator has a form:

$$m_0^2 = \frac{\mathbf{V}^T\mathbf{PV}}{n - m + d} \tag{11}$$

Calculation mean errors of the coordinates were conducted in a similar to the classical method, however the covariance matrix of adjustment estimated parameters, has in a free adjustment following form (SZUBRYCHT, WIŚNIEWSKI 2004, WIŚNIEWSKI 2005).

$$\mathbf{C}_{\hat{\mathbf{X}}} = m_0^2\mathbf{P}_{\tilde{\mathbf{X}}}^{-1}\mathbf{B}^T(\mathbf{B}\mathbf{P}_\mathbf{X}^{-1}\mathbf{B}^T)^{-1}\mathbf{A}_r^T\mathbf{P}\mathbf{A}_r(\mathbf{B}\mathbf{P}_\mathbf{X}^{-1}\mathbf{B}^T)^{-1}\mathbf{B}\mathbf{P}_{\tilde{\mathbf{X}}}^{-1} \tag{12}$$

In the robust free adjustment, particular importance has covariance matrix of the increments assuming erroneous of the approximate coordinates vector $\mathbf{C}_{\hat{\mathbf{X}}(zb)}$. Taking into account that $d\hat{\mathbf{X}}$ and $\mathbf{X}^0$ are two independent random variables in the vector $\hat{\mathbf{X}} = \mathbf{X}^0 + d\hat{\mathbf{X}}$, we can derive the formula of covariance matrix $\mathbf{C}_{\hat{\mathbf{X}}(zb)}$ for $m_0 = 1$ (WIŚNIEWSKI 2005):

$$\mathbf{C}_{\hat{\mathbf{X}}(zb)(\boldsymbol{m}_0=1)} = \mathbf{C}_{\mathbf{X}^0}\mathbf{B}^T(\mathbf{B}\mathbf{P}_{\mathbf{X}}^{-1}\mathbf{B}^T)^{-1}\mathbf{B}\mathbf{P}_{\bar{\mathbf{X}}}^{-1} + \mathbf{C}_{\hat{\mathbf{X}}} \tag{13}$$

where $\mathbf{C}_{\mathbf{X}^0} = m_0^2\mathbf{P}_{\bar{\mathbf{X}}}^{-1}$, is the covariance matrix of the vector of the approximate coordinates $\mathbf{X}^0$. The diagonal values of the matrix $\mathbf{C}_{\hat{\mathbf{X}}(zb)(m_0=1)}$, are mean squared errors of the adjusted estimates.

Robust free adjustment

The ideas of robust free adjustment are location and reduction the influence of outlying increments to geodetic coordinate of the points. The location of such coordinates in case of an gross error is not difficult. In free geodetic network occurs significantly increase value of coordinates increments burdened by gross error in relation to other increments. Reducing outliers increments in similar to the robust M – estimations (KAMIŃSKI, WIŚNIEWSKI 1992a, 1992b), is conducted by using damping of weight matrix, in our case weight matrix of coordinates $\mathbf{P}_{\mathbf{X}}$ (WIŚNIEWSKI 2005). For this purpose, we can applied one of the damping functions, such as Huber, Hampel or Danish function (KAMIŃSKI, WIŚNIEWSKI 1992a, 1992b, WIŚNIEWSKI 2005). In this study Danish damping function was used to increments $d\mathbf{X}$ and $d\mathbf{Y}$ as result we have following form (KAMIŃSKI, WIŚNIEWSKI 1992a, 1992b, KRARUP, KUBIK 1983):

$$t_X(d\overline{X}) = \begin{cases} 1 & \text{for } d\overline{X} \in \Delta_X = \langle -k_X; k_X\rangle \\ \exp\{-l_X(|d\overline{X}| - k_X)^{g_X}\} & \text{for } |d\overline{X}| > k_X \end{cases} \tag{14}$$

$$t_Y(d\overline{Y}) = \begin{cases} 1 & \text{for } d\overline{Y} \in \Delta_Y = \langle -k_Y; k_Y\rangle \\ \exp\{-l_Y(|d\overline{Y}| - k_X)^{g_Y}\} & \text{for } |d\overline{Y}| > k_Y \end{cases} \tag{15}$$

where:
$d\overline{X}$ – standardized increment for coordinate X,
$d\overline{Y}$ – standardized increment for coordinate Y,
$\Delta_X = \langle -k_X; k_X\rangle$ – acceptable range for standardized increments $d\overline{X}$,
$\Delta_Y = \langle -k_Y; k_Y\rangle$ – acceptable range for standardized increments $d\overline{Y}$,
l_X, l_Y, g_X, g_Y – control parameters.

Free robust adjustment solution is iterative. The first point of this process is to calculate the free increments $d\hat{\mathbf{X}}$ according to equation (10), and their covariance matrix in the form (13). On this basis standardized increments are calculated:

$$d\overline{\hat{X}}_j = \frac{d\hat{\mathbf{X}}_j}{m_{\hat{\mathbf{X}}_j}}, \quad d\overline{\hat{Y}}_j = \frac{d\hat{\mathbf{Y}}_j}{m_{\hat{\mathbf{Y}}_j}} \tag{16}$$

where $m_{\hat{\mathbf{X}}_j}$, $m_{\hat{\mathbf{Y}}_j}$ are mean errors of the estimators $d\hat{\mathbf{X}}_j$, $d\hat{\mathbf{Y}}_j$ (square root of suitable elements of the matrix $\hat{\mathbf{C}}_{\hat{\mathbf{X}}(zb)(\boldsymbol{m}_0=1)}$). Basis on value (16) and dumping function (14) and (15), equivalent weight matrix of increments vectors $d\hat{\mathbf{X}}$ is calculated. Denoting this matrix by $\hat{\mathbf{P}}_{\mathbf{X}}$, we can write:

$$\hat{\mathbf{P}}_{\mathbf{X}} = \mathbf{P}_{\mathbf{X}}\mathbf{T}(d\overline{\hat{\mathbf{X}}}) \tag{17}$$

where:

$$\mathbf{T}(d\overline{\hat{X}}) = \mathrm{Diag}\,\{t_X(d\overline{\hat{X}}_1),\ t_Y(d\overline{\hat{Y}}_1),\ldots,\ t_X(d\overline{\hat{X}}_{n_p}),\ t_Y d\overline{\hat{X}}_{n_p})\} \tag{18}$$

is diagonal damping matrix. If all standardized increments $d\hat{\mathbf{X}}_j$, $d\hat{\mathbf{Y}}_j, j = 1,\ldots,n_p$, are in their acceptable ranges (they are random), then the damping matrix $\mathbf{T}(d\overline{\hat{\mathbf{X}}})$ is the unit matrix. Afterwards we get $\hat{\mathbf{P}}_{\mathbf{X}} = \mathbf{P}_{\mathbf{X}}$ which ends the adjustment process. Otherwise, the next step is the iteration, in which vector of free increments is recalculated

$$d\hat{\mathbf{X}} = -\hat{\mathbf{P}}_{\mathbf{X}}^{-1}\mathbf{B}^T(\mathbf{B}\hat{\mathbf{P}}_{\mathbf{X}}^{-1}\mathbf{B}^T)^{-1}\mathbf{A}_r^T\mathbf{P}\mathbf{L} \tag{19}$$

with covariance matrix

$$\mathbf{C}_{\hat{\mathbf{X}}(zb)(m_0=1)} = \hat{\mathbf{C}}_{\mathbf{X}^0}\mathbf{B}^T(\mathbf{B}\hat{\mathbf{P}}_{\mathbf{X}}^{-1}\mathbf{B}^T)^{-1}\mathbf{B}\hat{\mathbf{P}}_{\mathbf{X}}^{-1} + \hat{\mathbf{C}}_{\hat{\mathbf{X}}} \tag{20}$$

Iterative process is continued so long until all the standardized increments will have values in their limits, respectively Δ_X and Δ_Y.

Characteristics of the geodetic test network

The first step was designed and staked out regular geodetic network, consisting five points on the area Kortowo II. The network have a shape of a square of side 200 [m] (Fig. 2). Network measurement was carried out in a single measurement session, obtained the observations presented in Figure 2.

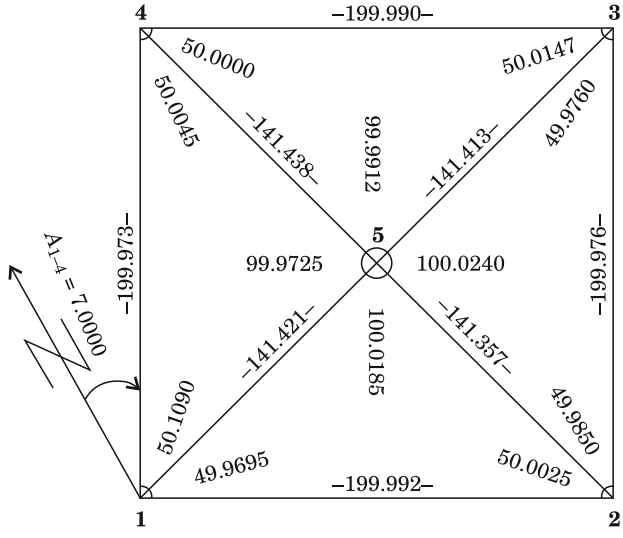

Fig. 2. The measurement results of the test network

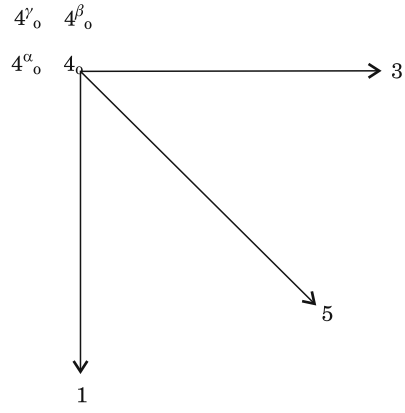

Fig. 3. The variants of the point no. 4 position

Let assume that the coordinates of the fourth point were contaminated by gross error. Then assumed that point as a fixed point during adjustment will have a negative influence on the obtained results of the adjustment. For the research purposes three variants of the position of the 4 (denoted by 4^{α}, 4^{β} and 4^{γ}) were designed, which simulate gross error in the coordinates (Fig. 3.). Values of the coordinates of point no. 4 are presented in Table 1. The aim of the research is to examine detecting of contaminated coordinates in the network by apply the robust free adjustment. Additionally the damping effect of

weights matrix of coordinates on the final results of the network adjustment will be examined. Displacement ΔX and ΔY will be treated as gross errors of the coordinates.

Table 1

The variants of the approximate coordinates of the point no. 4

Δ	Variant		
	4^{α}	4^{β}	4^{γ}
ΔX[m]	$\Delta X^{\alpha} = 0.00$	$\Delta X^{\beta} = 0.30$	$\Delta X^{\gamma} = 0.31$
ΔY[m]	$\Delta Y^{\alpha} = 0.30$	$\Delta Y^{\beta} = 0.00$	$\Delta Y^{\gamma} = 0.24$

Based on data from measurements approximate coordinates of pointsin the local coordinate system were calculated. To calculate the approximate coordinates, let assume following coordinates of point no. 1 $X = 1000$ [m], $Y = 1000$ [m] and azimuth $A_{1\text{-}4} = 7.0000^{[g]}$. Obtained, approximate coordinates are shown in Table 2.

Table 2

Summary of approximate coordinates

	No. point	1	2	3	4	4^{α}	4^{β}	4^{γ}	5
Computed approximate coordinates	X[m]	1,000.00	978.09	1,176.83	1,198.76	1,198.80	1,199.05	1,199.09	1,088.39
	Y[m]	1,000.00	1,198.79	1,220.74	1,021.94	1,021.65	1,021.98	1,021.71	1,110.40

Results of robust free adjustment

The results of robust free adjustment are the estimates of increments to the approximate coordinates of all points. The test network was adjusted freely for all of the four variants of the approximate coordinates. The network was adjusted for following means errors $m_k = 35^{cc}$, $m_d = 0.025$ [m]. The results of such adjustment are summarized in Table 3.

These results show a clear difference between the received estimates of parameters. In case of the classical adjustments, establishing the 4^{α} 4^{β} or 4^{γ} as a fixed point, cause that the results of the adjusted coordinates are even more distorted. In free robust adjustment Danish damping function was used. In the acceptable ranges $\Delta_X = < -k_X; k_X >$ and $\Delta_Y = < -k_Y; k_Y >$ for standardized increments $d\overline{X}$ and $d\overline{Y}$, was taken $k_X = k_Y = 1$. Then, with the probability equal 0.68 can be said that standardized increments which do not belong to the acceptable ranges are called outliers increments. In process of robust free

Table 3

Results of the classical free adjustment

No. point	Variant			
	I	II	III	IV
$\hat{X}_1$ [m]	1,000.00	999.97	1,000.10	1,000.07
$\hat{Y}_1$ [m]	1,000.00	999.98	999.98	999.95
$\hat{X}_2$ [m]	978.07	978.10	978.09	978.13
$\hat{Y}_2$ [m]	1,198.79	1,198.77	1,198.76	1,198.74
$\hat{X}_3$ [m]	1,176.85	1,176.90	1,176.86	1,176.91
$\hat{Y}_3$ [m]	1,220.72	1,220.63	1,220.76	1,220.68
$\hat{X}_4$ [m]	1,198.77	1,198.74	1,198.86	1,198.84
$\hat{Y}_4$ [m]	1,021.95	1,021.86	1,022.00	1,021.91
$\hat{X}_5$ [m]	1,088.39	1,088.40	1,088.45	1,088.46
$\hat{Y}_5$ [m]	1,110.40	1,110.35	1,110.41	1,110.36

adjustment, let assume the following parameters $g_X = g_Y = 2$ and $l_X = l_Y = 0.6$. Such a strict qualification has the relation to main aim, namely the effective identification of point displacement. Robust free adjustment is iterative. In the first step we assumed that the weight matrix of increment vector $d\mathbf{X}$ as the unit matrix. Therefore starting step is classical free adjustment is with optimization criterion $d\mathbf{X}^T\mathbf{P}_\mathbf{X}d\mathbf{X} = d\mathbf{X}^Td\mathbf{X} = \min$. Then $d\mathbf{X}^{(0)} = d\hat{\mathbf{X}}$, and next $d\overline{X}^{(0)} = d\widetilde{X}$. In each next step, the j-th iteration matrix of weights $\mathbf{P}_\mathbf{X}$ is replaced by the equivalent matrix $\hat{\mathbf{P}}_\mathbf{X}^{(j)} = \mathbf{P}_\mathbf{X}^{(j-1)}\mathbf{T}(d\overline{X}^{(j-1)})$, where $\mathbf{T}(d\overline{X}^{(j-1)})$ is diagonal

Table 4

Results of the robust free adjustment

Specification	Variant					
	II		III		IV	
	$\hat{\mathbf{X}}$	$d\hat{\mathbf{X}}$	$\hat{\mathbf{X}}$	$d\hat{\mathbf{X}}$	$\hat{\mathbf{X}}$	$d\hat{\mathbf{X}}$
$\hat{X}_1$ [m]	1,000.01	0.01	1,000.04	0.04	1,000.01	0.01
$\hat{Y}_1$ [m]	1,000.00	0.00	1,000.00	0.00	1,000.00	0.00
$\hat{X}_2$ [m]	978.07	-0.02	978.07	-0.02	978.08	-0.01
$\hat{Y}_2$ [m]	1,198.78	-0.01	1,198.78	-0.01	1,198.78	-0.01
$\hat{X}_3$ [m]	1,176.86	0.03	1,176.85	0.02	1,176.86	0.03
$\hat{Y}_3$ [m]	1,220.71	-0.03	1,220.74	0.00	1,220.71	-0.03
$\hat{X}_4$ [m]	1,198.77	**-0.03** ΔX = 0.00	1,198.80	**-0.25** ΔX= <u>-0.30</u>	1,198.78	**-0.31** ΔX = <u>-0.31</u>
$\hat{Y}_4$ [m]	1,021.94	**0.29** ΔY = <u>0.30</u>	1,021.98	**0.00** ΔY = <u>0.00</u>	1,021.94	**0.23** ΔY = <u>0.24</u>
$\hat{X}_5$ [m]	1,088.40	0.01	1,088.41	0.02	1,088.40	0.01
$\hat{Y}_5$ [m]	1,110.40	0.00	1,110.41	0.01	1,110.39	-0.01

damping matrix. After ten iterative steps, the following results of robust free adjustment were obtained.

The results of the computations clearly show which coordinates of the points are contaminated by gross terror. Of course, the method is the most effective for single outlying point in the network. With a greater number of contaminated points, their detection would be difficult or even impossible. The coordinates obtained in robust free adjustment were compared with the coordinates obtained in the classical free adjustment (variant I in Tab. 3.). The results of this comparison including the differences between the respective coordinates are summarized in Table 5.

Table 5

Summary of differences adjustment of network coordinates

Specification	$\hat{X}_1$ [m]	$\hat{Y}_1$ [m]	$\hat{X}_2$ [m]	$\hat{Y}_2$ [m]	$\hat{X}_3$ [m]	$\hat{Y}_3$ [m]	$\hat{X}_4$ [m]	$\hat{Y}_4$ [m]	$\hat{X}_5$ [m]	$\hat{Y}_5$ [m]
$\hat{\mathbf{X}}_{II} - \hat{\mathbf{X}}_I$	0.01	0.00	0.00	-0.01	0.01	-0.01	0.00	-0.01	0.01	0.00
$\hat{\mathbf{X}}_{III} - \hat{\mathbf{X}}_I$	0.04	0.00	0.00	-0.01	0.00	0.02	0.03	0.03	0.02	0.01
$\hat{\mathbf{X}}_{IV} - \hat{\mathbf{X}}_I$	0.01	0.00	0.01	-0.01	0.01	-0.01	0.01	-0.01	0.01	-0.01

The largest differences occur between the results of the classical free adjustment and the results of the robust free adjustment in III variant (for point 4 with approximate coordinates 4^{β}). Let consider a situation when in network, besides outlying points exist also observations contaminated by gross error. For the purpose of numerical example, an observation d1-4 was contaminated by gross error 0.400 m ($d_{1\text{-}4}$ = 199.573 m). The adjustment is conducted according to principles of hybrid M – estimation (CZAPLEWSKI 2004). This method is characterized by the simultaneous damping weights of observation weight matrix and damping weights of coordinates weight matrix. Therefore, besides the standardized increments the standardized corrections is determined.

$$\overline{\hat{\mathbf{V}}}_i = \frac{\mathbf{V}_i}{m_{\hat{\mathbf{V}}_i}}, \qquad i = 1,2,..., 20 \tag{21}$$

To determine these standardize corrections, it is necessary to specify the form of the covariance matrix of the corrections vector $\hat{\mathbf{C}}_{\mathbf{V}}$. The values on the diagonal on the covariance matrix are the squares of the mean errors of corrections. The covariance matrix of the corrections vector derivation is presented in the paper (CZAPLEWSKI 2004). Below the final form of covariance matrix of the corrections vector is presented:

$$\hat{\mathbf{C}}_{\mathbf{V}} = m_0^2 \mathbf{M}_+ (\mathbf{A}\mathbf{P}_{\mathbf{X}}^{-1}\mathbf{A}^T + \mathbf{P}^{-1})\mathbf{M}_+^T \tag{22}$$

where

$$\mathbf{M}_+ = \mathbf{I} - \mathbf{A}\mathbf{P}_{\mathbf{X}}^{-1}\mathbf{B}^T(\mathbf{B}\mathbf{P}_{\mathbf{X}}^{-1}\mathbf{B}^T)^{-1}\mathbf{A}_r^T\mathbf{P} \tag{23}$$

To identify and reduce the influence of observation contaminated by gross errors, the same value of parameters g, l and k as in the identification process of contaminated coordinates of the points is used. The adjustment procedure is analogous like in the previous example. In this case two equivalent weights matrices: $\hat{\mathbf{P}}_{\mathbf{X}}$ and $\hat{\mathbf{P}}_{\mathbf{X}}^{(j)} = \hat{\mathbf{P}}_{\mathbf{X}}^{(j-1)}\mathbf{T}(\mathbf{L}^{(j-1)})$, where $\mathbf{T}(\mathbf{L}^{(j-1)})$ is diagonal damping matrix are determined. After ten iterative steps, obtained the following results of geodetic network adjustment by applying hybrid M – estimation.

Table 6

The results of robust free adjustment (hybrid M – estimation)

Specification	Variant					
	II		III		IV	
	$\hat{\mathbf{X}}$	$d\hat{\mathbf{X}}$	$\hat{\mathbf{X}}$	$d\hat{\mathbf{X}}$	$\hat{\mathbf{X}}$	$d\hat{\mathbf{X}}$
$\hat{X}_1$ [m]	1,000.01	0.01	1,000.03	0.03	1,000.00	-0.00
$\hat{Y}_1$ [m]	1,000.00	0.00	1,000.00	0.00	1,000.00	0.00
$\hat{X}_2$ [m]	978.08	-0.01	978.07	-0.02	978.07	-0.02
$\hat{Y}_2$ [m]	1,198.78	-0.01	1,198.78	-0.01	1,198.78	-0.01
$\hat{X}_3$ [m]	1,176.86	0.03	1,176.85	0.02	1,176.85	0.02
$\hat{Y}_3$ [m]	1,220.72	-0.02	1,220.75	0.01	1,220.72	-0.02
$\hat{X}_4$ [m]	1,198.77	**-0.03**	1,198.79	**-0.26**	1,198.77	**-0.32**
$\hat{Y}_4$ [m]	1,021.94	**0.29**	1,021.97	**-0.01**	1,021.94	**0.23**
$\hat{X}_5$ [m]	1,088.39	0.00	1,088.40	0.01	1,088.39	-0.00
$\hat{Y}_5$ [m]	1,110.39	-0.01	1,110.41	0.01	1,110.40	-0.00

The results of the computations clearly show, that the coordinates were contaminated by gross error. Similar to the free robust adjustment, with an increasing number of observation contaminated by gross errors, it is more difficult to identified the contaminated points. It should be noted, that quantities of outliers are not the only problem with regard to the identification of outliers points. Unfortunately, this method is most effective in case of large errors in approximate coordinates.

Table 7

Results of the robust free adjustment

Specification	Variant									
	V		VI		VII		VIII		IX	
	$\hat{\mathbf{X}}$	$d\hat{\mathbf{X}}$	$\hat{\mathbf{X}}$	$d\hat{\mathbf{X}}$	$\hat{\mathbf{X}}$	$d\hat{\mathbf{X}}$	$\hat{\mathbf{X}}$	$d\hat{\mathbf{X}}$	$\hat{\mathbf{X}}$	$d\hat{\mathbf{X}}$
$\hat{X}_1$ [m]	1,000.00	0.00	1,000.01	0.01	1,000.01	0.01	1,000.01	0.01	1,000.02	0.02
$\hat{Y}_1$ [m]	1,000.00	0.00	1,000.00	0.00	1,000.00	0.00	1,000.00	0.00	1,000.00	0.00
$\hat{X}_2$ [m]	978.07	-0.02	978.07	-0.02	978.07	-0.02	978.07	-0.02	978.07	-0.02
$\hat{Y}_2$ [m]	1,198.79	0.00	1,198.79	-0.00	1,198.79	0.00	1,198.79	0.00	1,198.79	0.00
$\hat{X}_3$ [m]	1,176.85	0.02	1,176.85	0.02	1,176.85	0.02	1,176.85	0.02	1,176.85	0.02
$\hat{Y}_3$ [m]	1,220.72	-0.02	1,220.72	-0.02	1,220.72	-0.02	1,220.72	-0.02	1,220.73	-0.01
$\hat{X}_4$ [m]	1,198.77	**0.00**	1,198.78	**-0.00**	1,198.78	**-0.01**	1,198.78	**-0.02**	1,198.78	**-0.03**
$\hat{Y}_4$ [m]	1,021.96	**0.01**	1,021.96	**0.01**	1,021.96	**0.01**	1,021.96	**0.01**	1,021.96	**0.01**
$\hat{X}_5$ [m]	1,088.39	0.00	1,088.39	0.00	1,088.40	0.01	1,088.40	0.01	1,088.40	0.01
$\hat{Y}_5$ [m]	1,110.41	0.01	1,110.41	0.01	1,110.41	0.01	1,110.41	0.01	1,110.41	0.01

For small changes in the approximate coordinates, the coefficients matrix **A** is changing very slightly and has little effect on the final value of the vector $d\hat{\mathbf{X}}$. Table 7. presents the results of the robust free adjustment obtained for following variants of approximate coordinates (variant V – X_4^0 = 119,877 and Y_4^0 = 1,021.95, variant VI – X_4^0 = 119,878 and Y_4^0 = 1,021.95, variant VII – X_4^0 = 119,879 and Y_4^0 = 1,021.95, variant VIII – X_4^0 = 119,880 and Y_4^0 = 1,021.95, variant IX – X_4^0 = 119,881 and Y_4^0 = 1,021.95).

Conclusions

Developing the estimation methods has a significant influence on geodesy and related sciences. Implementation new computational algorithms, engineers gain new opportunities for solution geodetic observation. In recent years the development concern methods of robust estimation for gross errors. In this paper we have shown that the practical importance has also robust free adjustment. Classical free adjustment is most commonly used to adjustment free realization network (or other special-purpose networks). Such adjustment allow for optimum fitting adjustment of network to approximate network (network with known approximate coordinates). It is also possible objective analysis of the accuracy, independent of the variant elimination degrees of freedom network. Robust free adjustment remains mentioned above features of classical free adjustment, however allows identifying of points whose coordinates are burdened with gross errors. The reason of such errors may be

different, for example, resulting from unrecognized displacements points of network. In our test network, values of movements were known. This enabled the evaluation of effectiveness of robust free adjustment. The paper shows very interesting properties of the hybrid M – estimation which concerned damping weight of observation weight matrix and damping weight of coordinates weight matrix. In each of analyzed variant, a single outlying point has been detected. Although the experiment was carried out successfully this method has some limitations of the approach with regard to practical applications. These limitations concern among others the values of errors of the approximate coordinates that need to be in the range of linearity for the coefficients of matrices **A**. Additionally, it should be noted that method presented in this paper is most effective in a situation where only one point is outlying. In the case of existing more than one outlying point in the network, the detection problems of these points may appear. Robust free adjustment can be further developed and detailed comparative analysis. This may particular apply selections of other damping function. Detailed research of this method should concern the reliability against a larger number observation and outlying points.

References

CZAPLEWSKI K. 2004. *Positioning with Interactive Navigational Structures implementation*. Annual of Navigation, 7.

DUCHNOWSKI R. 2010. *Median-Based Estimates and Their Application in Controlling Reference Mark Stability*. Journal of Surveying Engineering, 136(2): 47–52.

HUBER P.J. 1981. *Robust Statistics*. Wiley, New York.

KAMIŃSKI W., WIŚNIEWSKI Z. 1992a. *Analiza wybranych, odpornych na błędy grube, metod wyrównania obserwacji geodezyjnych. I. Założenia*. Geodezja i Kartografia, XLI(3–4): 173–182.

KAMIŃSKI W., WIŚNIEWSKI Z. 1992b. *Analiza wybranych, odpornych na błędy grube, metod wyrównania obserwacji geodezyjnych. II. Analiza*. Geodezja i Kartografia, XLI(3–4): 183–195.

KRARUP T., KUBIK K. 1983. *The Danish Method; experience and philosophy. Deutsche Geodätische Kommission bei der Bayerischen Akademii der Wissenschaf*. Reihe A, Heft 7: 131–134.

RAO C.R. 1973. *Linear statistical inference and its applications*. John Wiley & Sons, New York.

SZUBRYCHT T., WIŚNIEWSKI Z. 2004. *Identyfikacja i poprawianie współrzędnych znaków nawigacyjnych obarczonych grubymi błędami wystawienia*. Zesz. Nauk. AMW w Gdyni, 1.

WIŚNIEWSKI Z. 2002. *Koncepcja metod opracowania wyników pomiarów nawigacyjnych*. AMW, Gdynia, Poland.

WIŚNIEWSKI Z. 2005. *Rachunek wyrównawczy w geodezji*. Wydawnictwo UWM, Olsztyn.

WOLF H. 1972. *Helmetrs Losung zum Problem der freien Netz mit singulorer Normalgleichundsmatrix*. ZfV, Heft, 5.

YANG Y.X. 1994. *Robust estimation for dependent observation*. Manuscr. Geod., 19(1): 10–17.

Technical Sciences 16(3), 2013, 193–209

GENERATING DATA IN UMP DATABASES TO PLANENERGY-SAVING ROUTES

Antoni Ligęza, Piotr Śliwa

Institute of Engineering
State Higher Vocational School in Nowy Sącz

Received 19 May 2013; accepted 22 July 2013; available on line 27 September 2013

K e y w o r d s: energy-saving route, bicycle routing, navigation, MTB, UMP, the power of a cyclist, cyclist, GIS, Garmin.

A b s t r a c t

In this article the model allowing finding energy-saving routes between two places in the navigation systems – for a cyclist's activity profile – was introduced. Preparing of the compiled routing maps for many kinds of navigation systems is possible by means of inclusion of model data into a database of UMP map project.

Introduction

Despite the fact that the satellite navigation systems where primarily made for car users, it is very common nowadays systems – so as to plan the optimal routes enabling to travel from one place to another – are also used by many other groups of users.

Finding an optimal route while analysing mainly its length (the shortest route) or the time of riding (the quickest route) does not show the amount of energy consumption needed to pass the given route in the appointed time. In normal conditions, in the traffic, there is invariably resistance of motion whose presence is not included in the satellite navigation systems. The most powerful shapes of resistance of motion are grade resistance (the gradient of the terrain) and air resistance.

Corespondence: Antoni Ligęza, Instytut Techniczny, Państwowa Wyższa Szkoła Zawodowa, ul. Zamenhofa 1a, 33-300 Nowy Sącz, phone: 18 547 29 07/08, e-mail: aligeza@pwsz-ns.edu.pl

The following units / people might be interested in planning energy-saving routes: those with limited reserves of energy (electricity or rock gas-powered vehicles [such stations are a rarity], scooter users, bicycle users and pedestrians) and car drivers who make use of petrol only to pass through the given distance and who consider a velocity not as the force associated with the aerodynamics but rather the force connected with a traffic jam.

Among the abovementioned groups of people – due to limited energy resources – a group of cyclists, who while taking long distances would like to cover them in the shortest time, has been appointed for the analysis. The truth is that the process of planning a bicycle trip from Hel (Poland) to Rome (Italy) can be an enormous challenge, but thanks to the developed model it can be much easier.

The choice of implementation environment of the energy-saving routes model

The process of implementation of the model that allows planning energy-saving routes among the most popular satellite navigation systems such as TomTom, Igo, AutoMapa, MapaMap or Garmin is absolutely impossible. Such an assertion is supported by the abovementioned firms themselves. The firm Garmin expresses its interest in a broader circle of customers (Garmin – Manuals, on line: http://www.garmin.com/us/support/). Apart from a car driver profile, Garmin implements the following profiles of activity: a car, a motorcycle, walking, trekking, a bicycle, recreational cycling, mountain cycling, a cross-country vehicle, a lorry. Initially, a happy customer, enjoying the fact that an adequate system has eventually been found, arrives at a conclusion that it simply does not work properly. The truth is that it cannot work since it is based upon a conventional approach that allows using only specific road types designed for a given activity profile. An extra function of planning routes – minimisation of acclivity and descent – was even implemented but, as it has been demonstrated in the subsequent phase of the given model, it is not adequate for minimisation of energy while covering a distance.

The analysis has been aimed at GIS Open Source projects. Out of two solutions under examination – OpenStreetMap and UMP (Prochowski 2008) – the latter has been appointed, mainly due to a high quality of data of the road network in Poland but also to its creators' plan to incorporate newly generated model data into existent databases, out of which the compiled routed maps are generated so as to be used at a variety of system platforms.

The current area of research and the accepted constraints on the energy-saving routes model

The current area of research includes a lot of studies analysing the process of cyclist activity routes planning. The papers (RAITH et al. 2009, RENDALL et al. 2012) present good reviews of actual tends into this issue. The main area of research is focused upon a qualitative analysis of a roadway while designing a route using a range of criteria in order to produce a score for a friendly routing.

However, studies attempting to analyse the process of energy-saving routes planning are lacking. This study, therefore, for the first time implements the model of energy-saving routes planning. This model has been formulated so as to facilitate the implementation into UMP map system, employing the currently available data. The layer of the roads network for cyclists will be selected from the whole roads of UMP network (by means of determining road attributes) ensuring a safe cycling (a cyclist does not have to pay attention to high traffic volumes, narrow roads and the lack of cycle paths). The formulated model takes into account the fact that the energy consumption needed for covering the section of a route will by influenced only by: (1) unchangeable, natural earthly conditions (for example, the impact of wind, precipitation, the state of the road surface, temporary traffic barriers have not been considered), (2) the bicycle rolling resistance, and (3) the aerodynamic resistance of a cyclist-bicycle set.

Energy-saving paths in a diagraph

The problem of planning the quickest, the shortest or the most energy-saving path from one place to another can be identified while considering a common problem of finding the shortest paths in a digraph $G = (P, K)$ the set of vertices P (*node*) with a set of nodes and the weight function $w: K \to \mathbf{R}$, assigning edges of weight of real values. The shortest path leading from a node u to a node v in a digraph G is a path traced from u to v, characterised by the fact that its weight is the lowest. This problem, in view of the notion of weight, can be identified as a way of finding the least "costly" path from one node to another. Localisation of the least "costly" path for the sake of expense of energy allows introducing a notion of energy-saving path. The weight function has to be specified for this path. For the shortest route the length of edges constitute its weights; for the fastest one edge length ratios do that in relation to, mainly, a mean velocity assigned to road types (FLINSENBERG 2004).

An object in motion is under the force that is a resultant of forces propelling and decreasing its motion. In terms of energy-saving process, it is essential to consider an influence of decreasing forces inhibiting motion that can be graphically shown in the shape of resistance to motion F_o. The force that has moved an object has produced work. And this work is assessed in relation to the time needed for its accomplishment. A velocity of an accomplishment of work specifies the power of unit (an engine, a person) P. An object has to have a dose of energy tantamount to amount of work so as to accomplish this work taking a specified route. It is easy to observe that a dose of energy needed for an accomplishment of work, while taking a route, has to be connected with the power of an object P. Accordingly, constant mean velocities, taken into consideration in context of the fastest routes, are replaced by the constant power P_c, that an object is certain to be supplied with in an existing environment while taking a specified route and adjusting a velocity of ride (more powerful resistance = a slower velocity of motion supported by a specified gearing in a power transmission system). A velocity of an object taking a specified route at constant resistance F_o, is expressed by means of the relation:

$$v = \frac{P_c}{F_o}$$

The weight of an edge at length d_i in a diagraph G expresses the time of passing a given route subject to resistance of motion, that is to say $w = \frac{F_o d_i}{P_c}$. For a planned route a sum of weights signifies the time in which a model object passes a given route maintaining the constant power P_c. For that reason the shorter time signifies the lower consumption of energy.

While planning the shortest routes are used road maps. On the strength of a map, in order to implement algorithms that allow planning an optimal path, a diagraph G must be employed. Edges of a diagraph are made of road segments – polylines that include, among others things, coordinates of points of a road curve, length, a road type, the name of road, an acceptable direction of traffic. The majority of those attributes is essential while planning routes. Nodes of a diagraph are marked in physical places of polyline intersections (e.g. the physical intersection of roads under and over a viaduct does not exist) or in places of connection of two polylines having different attributes (e.g. a soil-surfaced road entering an asphalt road).

A model of a cyclist's ride

Shapes of motion resistance

While in motion a cyclist has to overcome main resistance F (ORZEŁKOWSKI 1998) that influences the energy consumption of motion:
resistance of a road

– rolling resistance (apart from frictional resistance in bearings and gear-shifts that are present while in motion)

– height difference resistance (+acclivity, -descent)
aerodynamic resistance
Model data are as follows:
M = 75 kg – the weight of a model cyclist,
m = 13 kg – the weight of a model bicycle MTB,
G – a combined weight of a cyclist and a bicycle,
V_c = 25 km/h – a velocity that a cyclist has to maintain, in a flat terrain, overcoming other forms of motion resistance,
P_c – the constant power that a cyclist has to generate while passing an entire route,
g = 9.81 m/s^2 – gravitational acceleration,

Weather conditions: no wind, atmospheric pressure of 1 standard atmosphere (atm), air temperature equals 20°C.

Rolling resistance is caused by the cooperation of a bicycle wheel tires and a road surface. The total power of rolling resistance F_t, acting on the rider-bike system is directly proportional to the weight of the system, and takes the form when riding on a road inclined at an angle α:

$$F_t = f_t \cdot G \cos\alpha = f_c(M + m) \cos\alpha \tag{1}$$

where f_t means the total rolling resistance coefficient. It depends mainly on a type and size of tires, tire pressure, speed (a velocity impact is not significant for the speed at V_c) and a type of surface.

Off-roading, on unpaved surfaces, requires overcoming much larger forces of rolling resistance than riding on hard surfaces. Approximate values of a rolling resistance coefficient (Garmin – Manuals, on line: http://www.garmin.com/us/support/) depending on a type of surface are shown in Table 1.

Tabele 1

Rolling resistance coefficients for a surface from UMP project where a cyclist can move

A type of road in UMP project	f_{UMP}	A type of surface	Values of a coefficient f	
			from	to
0×3, 0×4, 0×5, 0×6, 0×7	0.015	asphalt and concrete surfaces	0.010	0.015
0×*a*	0.050	hard soil-surfaced roads	0.030	0.100
Not considered	0.150	wet gritty roads	0.080	0.150
0×16, {4×4}	0.100	hiking trails, firm ground, sand, pebbles	0.030	0.150

f_{UMP} – set value of rolling resistance coefficient for road types in UMP project.

On the basis of ERNEST (2010) it is accepted that f_c, on the assumption that $f = 0.015$, for the asphalt road surface. In consideration of a road type in forms of rolling resistance taken from UMP project, an applied dependence on a rolling resistance coefficient is gained:

$$f_c = 0.035 + f_{UMP} \tag{2}$$

Terrain height difference resistance – resistance of a hill, acting when driving uphill, is the main component of road resistance which, unlike rolling resistance is variable in different terrains and significantly affects an energy expenditure needed to pass through that segment of a route. Assuming a constant slope of a road surface, a positive angle α, as a slope of acclivity, and a negative angle while descending – the resistance force directed parallel to a road surface can be worked out from the formula:

$$F_h = G \sin\alpha = G \frac{\Delta h}{\sqrt{\Delta h^2 + d_p^2}} \tag{3}$$

with a height difference Δh between the end and the beginning of a segment of a road with a horizontal length d_p. For example, for the section of the road {(N49.47399 E20.55720), (N49.47843 E20.55255)} a 0×7 type, a height difference equals 60 m, $d_p = 580$ m, and for that reason $F_h = 100$ N.

While combining the power of terrain height difference and rolling resistance, one can employ the concept of *road resistance* (PROCHOWSKI 2008):

$$F_d = F_t + F_h = Q(f_c \cos\alpha + \sin\alpha) = Qf_\alpha \tag{4}$$

where f_α is the coefficient of road resistance. It allows revealing, globally, the impact of a road on the following system: a cyclist – a bicycle.

Aerodynamic resistance – the force of air resistance F_p is determined by means of the formula (PIECHNA 2000):

$$F_p = c_x A \, \rho \frac{v^2}{2} a_e v^2 \tag{5}$$

where: A – the frontal projection of the face of a bicycle and a cyclist, in the position occupied while driving; ρ – density of the air, c_x – the aerodynamic resistance coefficient, treating quantitatively aerodynamic properties of a cyclist on a bicycle and a bicycle itself; $v\left[\frac{\text{m}}{\text{s}}\right]$ – the relative velocity of a cyclist in relation to the air.

On the basis of, among other things, the research carried out by the author of the study: $\rho = 1.2 \frac{\text{kg}}{\text{m}^3}$, $A = 1.5 \text{ m} \cdot 0.3 \text{ m} = 0.45 \text{ m}^2$, $c_x = 0.98$ (a top coefficient has been accepted, corresponding to the given shape of a cyclist and a typical sport outfit. It differs significantly from a professional cyclist coefficient, which can on average be $c_x = 0.25$), and for that reason

$$F_p = a_e \, v^2 = 0.02 \, v^2 \frac{\text{km}^2}{\text{h}^2} = 0.2646 \, v^2 \frac{\text{m}^2}{\text{s}^2} \tag{6}$$

At a speed of 10 km/h, the air resistance force equals 2 N. The process of doubling of a velocity makes the resistance force four times bigger, for a velocity of 25 km/h it takes the value of 12.5 N, the equivalent resistance of ascension during the acclivity on a surface inclined at an angle of circa 0.8° to the level.

The power increase of strength of air resistance can be illustrated by means of an example (ERNEST 2010), demonstrating that with an uninhibited descend on a road inclined at an angle of 5°, a cyclist is able to reach a maximum velocity of 70 km/h, at that point the equilibrium between road resistance and air resistance occurs. The air hinders one's motion, preventing a cyclist from reaching a higher velocity.

Windy weather conditions

A violation, adopted in section *Shapes of motion resistance*, of the assumption about a windless weather can completely change the fact of the energy

consumption of a planned route. Assuming a wind velocity higher than 0, parallel to the direction of motion v_α, with a positive value for the opposite wind and a velocity of a cyclist in regard to the ground v_g, we will achieve the previously introduced force of air resistance in the following shape

$$F_p = a_e\, v^2 = a_e\, (v_g \pm v_2)^2 \tag{7}$$

Maintaining a velocity of 25 km/h against the wind of, e.g., 30 km/h requires a cyclist to overcome five times the given resistance, namely 60 N. It is difficult to meet the assumption of maintaining a constant power of a cyclist.

Will it be ever possible to include the strength and direction of the wind in the model? Routable maps taken from UMP project are compiled daily and the possibility of taking into account those pieces of information is recognised while using the available map of wind gradient. The data would thus have only one-day validity. But there are other problems, such as the multiple-day routes and the fulfilment of the assumption that the wind strength and direction will be constant all the time. This assumption will never be fulfilled. Hence, the justification for the assumption of windless weather conditions, and only under such conditions the energy-saving routes in UMP will be planned.

A model velocity of a cyclist

Motion resistance affects an energy expenditure of a cyclist, essential to pass the given road at a certain time. Depending on the power of resistance, a cyclist passes equally long sections of a road reaching different velocities because a body's capacities, while providing more power to maintain a constant velocity at high resistance power, are very limited, unlike in motor vehicles case. Therefore a cyclist, on a given route, cannot maintain a constant velocity – only the constant power. The value of the constant power is determined for a middle class cyclist who along the whole route can maintain, on a model MTB bicycle, a constant velocity v_c, in a flat area, using an asphalt road ($f_c = 0.05$), beating other forms of motion resistance:

$$P_c = Fv_c = (F_t + F_p)v_c = 119 \text{ W} = 0.162 \text{ KM} \tag{8}$$

A velocity in km/h which must be maintained so as to achieve the power P_c, is a real root v_1 of an equation:

$$P_c = 3.6^{-3}\, a_e v^3 + 3.6^{-1}(F_t + F_h)v$$

$$v_1 = 3.6 \left(\frac{\sqrt[3]{2}(F_h + F_t)}{\sqrt[3]{27a_e^2P_c + \sqrt{108a_e^3(F_h + F_t)^3 + 729a_e^4P_c^2}}} + \right.$$

$$\left. + \frac{\sqrt[3]{27a_e^2P_c + \sqrt{108a_e^3(F_h + F_t)^3 + 729a_e^4P_c^2}}}{3\sqrt[3]{2}a_e} \right) \text{[km/h]} \qquad (9)$$

The following chart shows the relationship v_1 between a velocity and the angle of the terrain gradient.

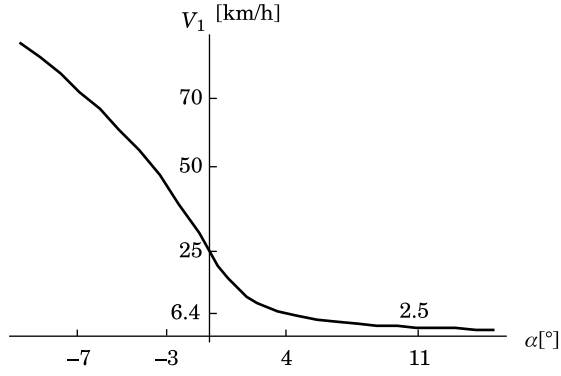

Fig. 1. Reliance of a velocity of a cyclist on terrain gradient for (f_c = 0.05)

For an acclivity at 11° gradient, for a cyclist to maintain the power P_c, one has to move slowly at 2.5 $\frac{\text{km}}{\text{h}}$. Riding below that velocity can cause a problem in maintaining the balance of a cyclist on a bicycle. In such a situation, one has to lead a bicycle; keeping up the pace of a walk at 2.5 $\frac{\text{km}}{\text{h}}$ with a bicycle is no longer any problem. It is assumed that a velocity equals:

$$\hat{v} = 2.5 \frac{\text{km}}{\text{h}} \text{ for } v_1 < 2.5 \qquad (10)$$

While a cyclist is descending, the situation is reversed. At a gradient of α = –3, a cyclist, can achieve a velocity of 50 $\frac{\text{km}}{\text{h}}$, and for a terrain descend

gradient –7 a velocity of 70 $\frac{\text{km}}{\text{h}}$. The last value is determined as a final one; above that velocity cycling becomes dangerous. A cyclist can have problems maintaining so high velocities on a curved road where the centrifugal force $F_r = \frac{(m + M)v^2}{R}$ occurs (with a momentary curvature radius of a road R). The maximum lateral force cannot be higher than the force of friction. The maximum velocity of a ride at the arc, in view of slipping wheels, can be calculated be means of the formula [0]: $v_{\max R} = \sqrt{\mu g R}$, where the tyre friction coefficient for a road μ takes values in the range from 0.2 for 0×a type to 0.8 for 0×1–0×6 types. Determination of a momentary radius of curvature for a road, marked with a string of points forming a polyline, is an easy analytical geometry task. However, in order to determine the maximum velocity of a cyclist, along the given route, it is not enough to limit only to $v_{\max R}$, which, at times, is not sufficient to limit the maximum velocity on the route similar to a straight line.

The solution would be usage of – used in many GPS navigation systems – the table of mean velocities which in line with a model solution will be used as the table of impassable velocities on specified road types (sample data are shown in the table 2).

Tabele 2

Impassable velocities of a cyclist on specified UMP road types

UMP road type	Maximum velocities
0×3,0×4,0×5	70
0×6	60
0×7	40
0×a,0×d	30
0×16	25

Justification for adopting such an approach lies in considering the fact that while designing a specific road type, designers must take into account velocities of moving vehicles; the process is reflected in appropriate profiles of road types.

A ride of a model cyclist – each cyclist passes through the given route differently, handling the various power distribution over time of a ride (FRIEL 2004). A cyclist generally attempts to maintain a steady velocity and does not pay attention to the fact that its continuation in the field with a slight assent causes more power consuming. A cyclist – the source of move – has different characteristics of the power delivery than a mechanical engine. Its uneven distribution over time leads to the fact that an initial fast driving, at the

further section of the route, may be reduced and frequent stops for regeneration of energy providing the specific power will be needed.

A model ride of a cyclist is different. It relies on the process of maintaining, while driving, a constant power, not a velocity (in a flat area a constant velocity equals 25 km/h). The time of crossing an entire route t_t consists of a travel time t_j and a waiting time t_p, needed for the recovery of energy. Depending on the condition, a model time of a ride is increased with a time t_p, testifying for a cyclist;s physical preparation. A model ride of a cyclist is characteristic of a long-distance cyclist who knows how to make a uniform distribution of force along an entire route, and for those people, these routes will be energy-saving.

For example, if a cyclist knows that he/she can maintain in a flat area a velocity of 25 km/h, by the time t_j = 3 h, covering thus 75 km (keeping a constant power all the time), then in the area of assent 3° in time t_j, and riding at a model velocity of 8.2 km/h, a cyclist will cross 24.6 km and a height difference of 3930 m. A future problem for a cyclist will be to assess how fast he/she needs to cross a section of a route because the navigation devices available now do not perform this function.

Implementation of a model in UMP project

UMP road network

UMP with its reach minutely models the Polish road network. The project covers the area of the whole world but its coverage is not as extensive as an analogous project OpenStreet.

A spatial database of UMP project is composed of PFM (Polish Format Map) text files (KOZICKI 2009), shown in view of the location and types of objects.

PFM has been developed by the author of the program cGPSmapper in order to create compiled maps used in Garmin receivers. The program has allowed making generalisations about the format by adding new data which will enable creation of compiled maps, used in various systems and applications (such as Android, iPhone, Windows Mobile, Symbian, Navitel, Garmin, WWW – http://mapa.ump.waw.pl, civic navigation http://jakdojade.pl). An extensive list of versions and applications can be found at: http://ump.fuw.edu.pl/wiki/Wersje.

The objects of road network used by a cyclist and shown in PFM format comprise sections entitled `polyline`. Below you can find an example of an entire Piramowicz Street in Nowy Sącz 0×5 type (a complex road). The

coordinates of the points of bends of the street, expressed in degrees in GPS system (width, length), will be taken only from 0 level, from `Data0`.

```
[POLYLINE]
Type = 0x5
Label=Piramowicz
EndLevel=2
Data0=(49.59984,20.68605),(49.59922,20.68718),(49.59913,20.68728),
(49.59905,20.68733),(49.59849,20.68763),(49.59839,20.68781),
(49.59832,20.68805),(49.59830,20.68833),(49.59833,20.68849),
(49.59836,20.68863),(49.59860,20.68915)
Numbers1=0,O,1,7,E,2,20
Numbers2=6,O,9,9,E,22,24
Plik=src\NOWY_SACZ.ulice.txt
[END]
```

In the `polyline` section you can add, after having arranged for it with the authors of UMP, new attributes that are necessary for implementation of a bicycle routing, based on the criterion of minimising the energy. For each `polyline`, object where a cyclist can move, it will be necessary to generate data for the `SpeedBike`, attribute with a model velocity of a cyclist riding in the direction from the first to the last point forming a polyline and in the opposite direction (e.g. `SpeedBike=10.2, 50.1` – a model cyclist, in the direction of moving, rides with a velocity of 10.2 $\frac{\text{km}}{\text{h}}$ (acclivity), and in the opposite direction (descend) with a velocity of 50.1 $\frac{\text{km}}{\text{h}}$). In order to achieve an adequate fit of a model to the actual terrain conditions – which may significantly differ from the assumptions – prevalent in particular road types (e.g. road signs reducing a velocity because of local dangers may occur, or for 0×16 type, while descending, it will not be possible to reach a high model velocity in view of a surface that prevents an uninhibited descend) it is necessary to introduce `SpeedBikeFix`, attribute that encodes the same velocity of a cyclist. Once the attribute is placed in `POLYLINE` section, `SpeedBike` velocities are ignored, giving way to real values.

A numerical terrain model – NTM

In order to determine F_h, resistances caused by terrain height difference, it is necessary to specify a terrain profile for each polyline. Prevalence of electronic computing technology has been responsible for a widespread use of, in a similar type of engineering tasks, numerical terrain models that mathematically portray a landform.

A numerical terrain model (NTM) of the Earth, created jointly by NASA and Japan, has been used to generate the data. It was created out of over a million stereomicroscopic pairs of images, collected by the Japanese ASTER (Advanced Spaceborne Thermal Emission Reflection Radiometer), the instrument located aboard the Terra satellite. NASA and the Japanese Ministry of Economy, Trade and Industry (METI) have developed a set of data which can be downloaded from the Internet for free.

The points of this terrain model comprise a regular grid of 30×30 m squares. For the area of Poland data has been downloaded from the website: http://gdex.cr.usgs.gov/gdex/ using ESRI GRID ASCII format, in seven parts, due to introduced restrictions on a single use download. ASTER Global DEM V2, ArcAscii, Projection has been chosen:

```
GEOGCS["GCS_WGS_1984",DATUM["D_WGS_1984",SPHEROID["WGS_1984",
6378137,298.257223563]],PRIMEM["Greenwich",0],UNIT["Degree",0.
0174532925199433295]].
```

Below there is a heading of one of downloaded spheres in ESRI GRID ASCII format:

```
ncols         16690
nrows         6407
xllcorner     18.984375000000
yllcorner     48.779314138406
cellsize      0.000277784901
NODATA_value –32768
284 281 279 276 275 277 282 281 ...
289 296 306 316 325 313 308 303 ...
.............................
```

In order to obtain data in one rectangular XY set, NTM ellipsoidal coordinates and polylines (`Data0`) have been transferred to the 1992 National Coordinating Centre using the formulas given in SNYDER (1987) for the Transverse Mercator map projection with accepted parameters: scale on the midpoint meridian $m_0 = 0.9993$, the midpoint meridian $\lambda_0 = 19^o$

Knowing the coordinates of the nodes of the grid of NTM squares, the height of any point $P1(x,y)$, located inside the $ABCD$ square (fig. 2), can be calculated by means of the following formula:

$$H_{p1} = r^{-2}[(r - \Delta x)(r - \Delta y)H_A + \Delta x(r - \Delta y)H_B + \Delta x\Delta y\, H_C + (r - \Delta x)\Delta y\, H_D]$$

$$\Delta x = x_{P1} - x_A;\ \ \Delta y = y_{P1} - y_A \tag{11}$$

where r is the length of the grid square; H_A, H_B, H_C, H_D being corner heights of its nodes.

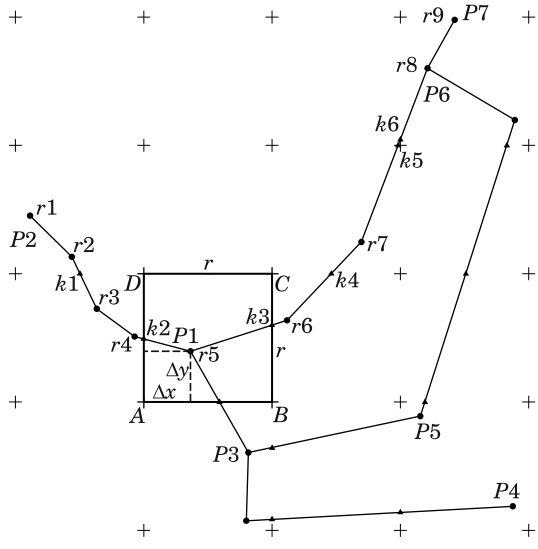

Fig. 2. UMP project road network with NTM square grid

An appointment of model velocities along any segment of a route

Let us consider a representative polyline taken from figure 2, with a known road type t, appointed by the points $r1$, ..., $r9$, whose coordinates have been previously transformed into the "1992" rectangular set. The polyline crosses the sides of the grid of NTM squares at the points $k1$, ..., $k6$ whose coordinates are likewise located in the "1992" set. As a result of crossing of the polyline through DTM, the height is assigned to each *ri, ki* point using the formula (10), creating a profile of a road out of ordered points, possessing now three coordinates (x, y, h):

$$S = (r1, r2, k1, r3, r4, k2, r5, k3, r6, k4, r7, k5, k6, r8, r9)$$

For each section of the profile $|s_i, s_{i+1}|(i = 1, ..., \bar{S} - 1)$ with a length d_i, a velocity is appointed using the dependence (9): v_{1i} – in a consistent direction and a return direction $|s_{i+1}, s_i|$, namely v_{i1}. The final values after considering the dependence (10) and the impassable values taken from table 2 are expressed by means of symbols $\hat{v}_{1i}$, $\hat{v}_{i1}$. The attribute value `SpeedBike` will be appointed from the following dependence:

$$\texttt{SpeedBike} = \frac{\Sigma d_i}{\Sigma \frac{d_i}{\hat{v}_{1i}}}, \frac{\Sigma d_i}{\Sigma \frac{d_i}{\hat{v}_{i1}}} \tag{11}$$

While creating linear objects in UMP project, an economic principle of drawing maximum long objects possessing fixed attributes (a label, a type, unidirectionality of a road, the level of visibility on a map, traffic restrictions – `ForceClass`) has been adopted. This leads to a necessity of extension of SpeedBike attribute value on account of the fact that after the road network from figure 2 has been transformed into the graph (fig. 3), determination of weights on the edges between nodes will be impossible: *P*2*P*1, *P*1*P*6, *P*6*P*7 weight for *P*2*P*7 edges.

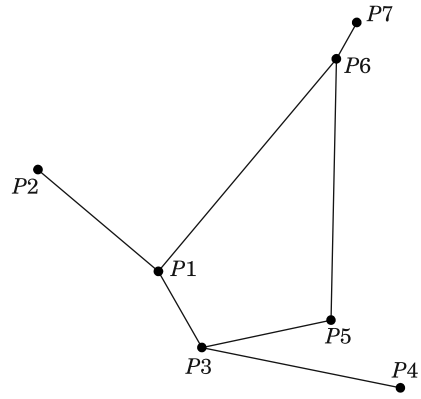

Fig. 3. The graph of road network, made from a section of UMP project, presented on figure 2

Prior to the process of determination of model velocities, a generating program finds nodal points, and along every section from a node to a node it sets values from (11). The process of encoding values on attributes, for polylines with i points, is as follows:

```
SpeedBike=5,18,30;8,10,45;9,25,25
SpeeBikeFix=8,12,21
;------------------------------
SpeedBike=5,18,30;8,10,45;9,25,25
SpeeBikeFix=5,12,16;9,15,20
```

The above entry signifies that starting from the point 1 to 5, a model velocity of a cyclist is 18 and 30 in return direction; between points 5–8 it is 10 and 45 respectively, and ending at the 8–9 edge with the velocity of 25, that is on the flat terrain. The introduction of actual values by `SpeeBikeFix`

attribute is not necessary for all edges. The abovementioned entry means determination of the velocity up to the point 8, from a nodal point located directly in front of it, namely the node 5.

Conclusions

The assignation of bicycle paths, based on the conventional models used in routes planning process for motor vehicles is, in the area of diverse terrain shapes, difficult to accept. In this paper, on the example of the activity profile of a cyclist, the model has been developed, enabling the process of planning of energy-saving routes that can be effectively used by various entities whose energy resources are limited due to physical limitations or rarity of places where the refilling of energy is possible. The given model takes into account the fact that the consumption of energy needed for crossing the given section of a route is affected only by: unchangeable, natural conditions of the earth, a bike rolling resistance and aerodynamic resistance of a cyclist-bicycle set.

Our choice of the cyclists – treated in the given article as a model group – was made in view of the desire to change the prevailing belief among them that the satellite navigation systems are unsuitable while planning optimal routes. A deeper analysis of the problem allowed us to find the causes of this situation. The shortest route in a corrugated terrain that could even be the fastest one – may demand from a cyclist more effort and time than an energy-saving route which may even be 5 km longer than the shortest route, the one of about 60 km. Car drivers do not need to pay greater attention to energy consumption of a route because they can dynamically increase the power input, maintaining a constant velocity, regardless of air resistance. Furthermore, it is hard to show competently what profit they could have as far as fuel consumption is taken into consideration while taking an energy-saving route. A middle class cyclist, however, has limited power resources at the level of tenths of a metric horsepower (KM) that do not allow a cyclist to maintain a constant velocity while riding in a "sinuous" terrain. Hence, the problem of usability of car navigation arises while planning routes for units with a low range of the power intake and a necessity to implement the developed energy-saving routing should be highlighted.

The developed model is set up to be implemented into UMP map project that allows one to add the necessary model data to your databases and create compiled maps with an energy-saving routing for a specific system platform (e.g. Garmin, Navitel or those with Android operating system, Symbian, Windows Mobile).

References

ERNEST K. 2010. *Fizyka sportu*. PWN, Warszawa.
FLINSENBERG I. 2004. *Route planning algorithms for car navigation*. TUE, Eindhoven.
FRIEL J. 2004. *Biblia treningu kolarza górskiego*. Buk Rower, Zielonka.
Garmin – Manuals: http://www.garmin.com/us/support/
KOZICKI S., TURNER G., BOWRING G., SCHEFFLER H., SHEPPARD K., RIKKER G., ZALBA M. 2009. *cGPSmapper User Manual*. On line: http://cgpsmapper.com (access: 27.09.2013).
ORZEŁKOWSKI S. 1998. *Budowa podwozi i nadwozi samochodowych*. WSiP, Warszawa.
PIECHNA J. 2000. *Podstawy aerodynamiki pojazdów*. WKŁ, Warszawa.
PROCHOWSKI L. 2008. *Mechanika ruchu*. WKŁ, Warszawa.
RAITH A., VAN HOUTTE C., WANG J.Y.T., EHRGOTT M. 2009. *Applying bi-objective shortest path methods to model cycle route-choice*. Proceedings of 32nd Australasian Transportation Research Forum, on line: http://www.cmsl.co.nz/assets/sm/4433/61/paper106-Raith.pdf (access: 27.09.2013).
RENDALL S., ROSE P., JANSSEN K. 2012. *Delivering effective cycle facilities: modelling bicycle route choice*. Institution of Professional Engineers New Zealand (IPENZ) Transportation Group Conference.
SNYDER J. 1987. *Map projection – a working manual*. USGPO, Washington.
UMP – mapa, on line: http://ump.waw.pl/ (access: 27.09.2013).

Technical Sciences 16(3), 2013, 211–220

BIOMASS AS A RENEWABLE SOURCE OF ENERGY

***Paulina Drożyner*[1], *Wojciech Rejmer*[1], *Piotr Starowicz*[2], *Andrzej Klasa*[3], *Krystyna A. Skibniewska*[1]**

[1]Chair of Foundations of Safety
[2]Chair of Food Biotechnology
[3]Chair of Agricultural Chemistry and Environmental Protection
University of Warmia and Mazury in Olsztyn

Received 27 May 2013; accepted 30 September 2013; available on line 30 September 2013

K e y w o r d s: biogas, methane, energy dedicated crops, renewable energy.

A b s t r a c t

In this paper state of art on known and potential biomass sources is reviewed. The review will consider energy dedicated crops and waste types that are already applied for clean energy purposes as well as potential ones. The resources can be applied for biofuels, bioethanol, methane, hydrogen production by means of various processes (methane fermentation, pyrolysys etc). The environmental and economical benefits of biomass application as a renewable energy source are also described.

Introduction

Rapid industrial progress has caused sudden increase of energy consumption. This phenomenon is especially visible in developing countries. Traditional methods of energy production were based on fossil fuels (mostly oil and gas), which caused consequences in form of excess emission of greenhouse gasses (ZIEMIŃSKI, FRĄC 2012). Industrial revolution and civilization development led to burdensome climactic changes. According to scientific research the 2°C rise of average temperatures can lead to extinction of plants and animals. Climate warming causes many environmental problems such as: floods, hurricanes, drought, tropical cyclones, erosion of coast beaches, increase of sea level (which leads to submersion of islands and lowlands), and problems in drinking water

Corespondence: Paulina Drożyner, Katedra Podstaw Bezpieczeństwa, Uniwersytet Warmińsko-Mazurski, ul. Heweliusza 10, 10-718 Olsztyn, phone: +48 89 524 56 12, e-mail: d.paulina@poczta.onet.pl

supply for humans and animals (SHUIT et al. 2009). In order to decrease the above climactic problems, consumption of fossil fuels and increase energy efficiency two types of actions were undertaken – development of energy saving programs, and research on renewable energy sources. Energy from renewable sources although more expensive in production then conventional energy has many advantages. It leads to reduction of carbon emission to atmosphere, it is compatible with rules of balanced development, it reduces the dependence on fossil fuels and is not as dangerous as atomic energy (BANOS et al. 2011). According to SAYNIGH (2012) we distinguish following renewable energy sources: solar radiation, wind, water and ocean currents, biomass, biofuels, geothermal sources and hydrogen.

Poland as a member of European Union is obligated to adjust to European energy policy. Currently the use of renewable energy in relation to other countries is insufficient. In *Energy from renewable sources 2011* (http://www.stat.gov.pl) report the predictions are that energy produced from renewable sources should be 15% of overall energy consumption until 2020. On Figure 1 the percentage of renewable sources energy consumption to overall usage in UE and in Poland in 2002-2010 period. It visualizes how far Poland is in comparison to UE countries considering renewable energy development.

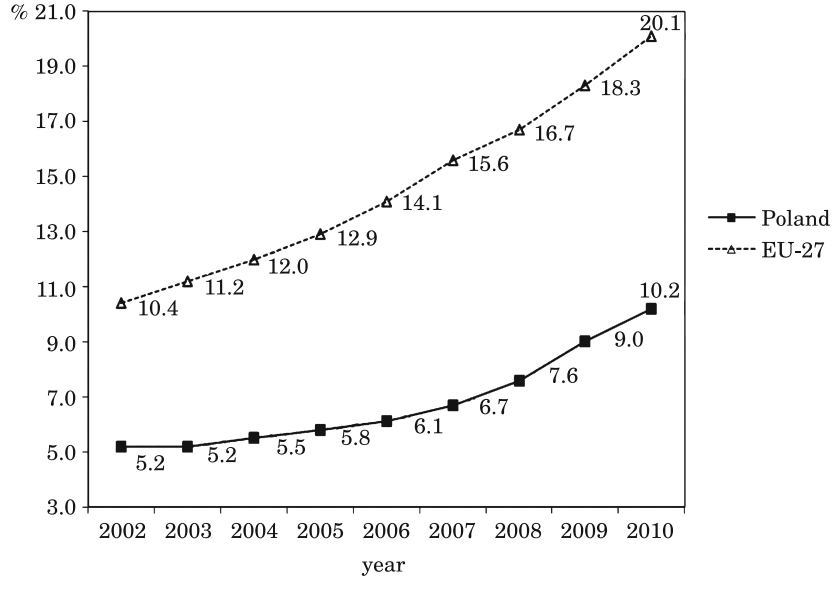

Fig. 1. Percent of energy obtained from renewable sources in UE and Poland in 2002–2010 period
Source: Główny Urząd Statystyczny. Portal Informacyjny, on line: http://www.stat.gov.pl/gus

Biomass as energy source

Biomass is one of the most promising alternative energy sources, because similar to that of carbon neutrality and availability from multiple sources (LIM et al. 2012). According article 2 of 25th of August 2006 law on biocomponents and liquid biofuels biomass consists of: solid or liquid substances of plant or animal origin, which undergo biodegradation from products, waste and leftovers of agricultural and forest production, and their products processing industry and parts of other wastes which undergo biodegradation, especially agricultural raw materials. According to DODIĆ et al. (2012) biomass after partial processing can be in solid state (briquettes, pellets), liquid (biodiesel, biomethanol and bioethanol) or gas (biogas, syngas and hydrogen). Since mastering fire biomass was used for energy production in burning process and has been used since then, especially in third world countries example: Tanzania or Ethiopia, where 90% of energy originates from biomass (KELLY-YONG et al 2007). The most favorable from the balanced development point of view is biomass processed to liquid fuels, because the highest energetic efficiency can be achieved this way (SUNTANA et al. 2009). Biomass can be processed by means of: thermo-chemical methods to liquid fuels, gasses (carbon oxides methane), or pyrolysis where hydrogen is the final product.

Biomass can be also processed by biotechnological means. Through fermentation of oily plants biodiesel is produced, which can be used in standard diesel

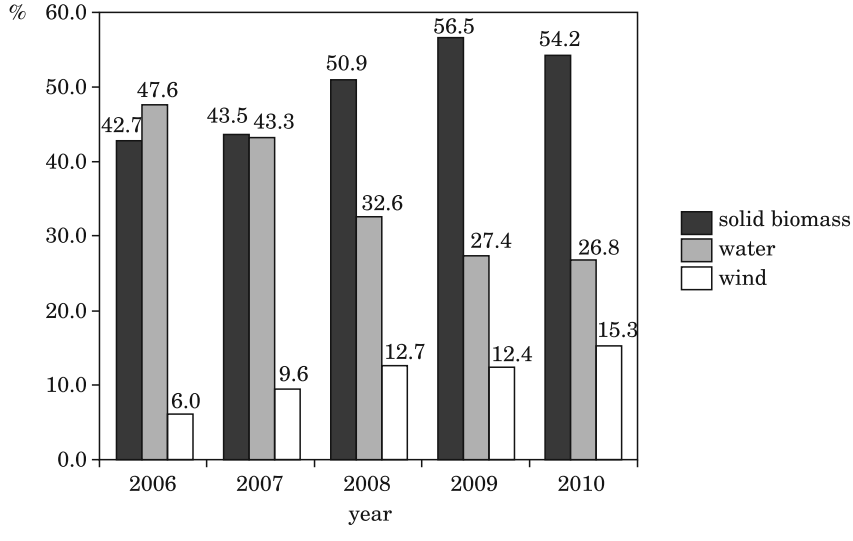

Fig. 2. The contribution of solid biomass, wind and water to electric energy in Poland in 2006–2010
Source: Główny Urząd Statystyczny. Portal Informacyjny, on line: http://www.stat.gov.pl/gus.

and gas engines, after minimal modifications. Through fermentation of municipal waste such as post breading waste exp. manure the biogas with relatively high content of methane can be obtained (ZAGORSKIS et al 2012). This proves high biomass potential as an energy source which can replace conventional fuels in the near future (DEMIRBAS 2008). Biomass is a clean renewable energy source, which can greatly improve the environment, economics and energetic security. Biomass application as an alternative energy source is beneficial for developing countries because of availability of local raw materials and employment of local labor for its production and processing (DEMIRBAS 2008).

In Poland biomass is getting more and more popular as electric energy source, and is dominant to water and wind energy (Figure 2).

Biomass main sources

Energy dedicated willow (*Salix viminalis*)

One of the more and more popular biomass types is energy dedicated willow. Two types are present in nature: tree type and bush type (more often used for energy production). It is characterized by high resistance to soil contaminations and quick growth (STOLARSKI 2003). Growth cycle of energy dedicated willow is 3 to 5 years, thanks to which it is considered a fast renewable source (TAHVANAINEN, RYTKONEN 1999). Its wood (unlike coal) does not emit green house gasses in burning process and is characterized by low emission of nitrogen, chlorine and sulfur to atmosphere. It has low accumulation of heavy metals from soil, which makes it ideal for energetic purposes (JAMA, NOWAK 2012). Application of energy dedicated willow for soil purification purposes is not an ideal solution. Though the elimination of excess nitrogen is satisfactory, the low soil purification in case of excess chlorine still remains a problem, especially in dry climate where concentration of this element may exceed toxic values (MARMIROLI et al. 2012).

Willow may find application in waste purification from small household waste water disposal facilities. Water purification is achieved through usage of nutrients from sewer sludge and simultaneous biomass for bioenergy production. Household wastewater is almost ideal nutrient for willow plantation fertilization. Part of the differences between plants need for nutrients and content of substances in wastes is neutralized by the soil. Household wastewater are more effective for fertilization because of lower concentration of heavy metals than in industrial wastewater, which can inhibit plant and soil microorganisms growth. Both of these processes lead to decrease of waste

utilization. Research on application of *Salix viminalis* grown on hydroponic gravel for waste utilization published by MANT et al.(2003) had shown that effectiveness of utilization of gravel alone is: 90% for BOD, 45.7% for nitrogen, 85.8% for phosphorus, and 6.9% for potassium. The plant increases this effectiveness of 12% for nitrogen and 5% and 18% for phosphorus and potassium.

JAMA and NOWAK (2012) investigated the application of energy dedicated willow for utilization of sewage sludge. They are considered as wastes of high organic compounds and nutrients concentration, thus good fertilizer material. Sewage sludge are a inhomogeneous material, dependent on waste type, applied technology and season of the year. Before application it needs to be checked for the presence of pathogenic bacteria. When energy dedicated willow is being fertilized it accumulates 20% of phosphorus in the first year and this amount increases in time. The same goes for nitrogen but the amounts of accumulated element differ with carried out research and vary from 20% (and increase to 25% in following years) to 70% in the first year. Willow also accumulates calcium (3.1%), magnesium (0.81%) and sulfur.

Wastes of freshwater fish breeding ponds are a great problem for breeders. A huge amount of water is needed in order to minimize the concentration of ammonium, which dissolves impurities from excrements and non digested leftovers. Wastes are mostly waters with small concentration of contaminants. A simple and ecological solution for waste utilization is watering of energy dedicated willow and poplar plantations, because of a their higher water usage in comparison to other types of trees. Research carried out in Canada in 2005 proved that willow and poplar can be intensively watered with water from breeding ponds and decrease the sewage phosphorus income to natural ecosystem (FILLION et al 2009).

Sweet sorghum (*Sorghum Moenh*)

It is a very promising plant for energy application. High photosynthesis efficiency, high resistivity to water deficit, small fertilizer need, ease of climactic and soil accommodation and high surface efficiency are its benefits. The growth period is 3-5 months long in warm climate conditions (MATSAKAS, CHRISTAKOPOULOS 2013, MEKI et al. 2013). Sorghum is energy dedicated plant attractive for bioethanol production, because of high sugar concentration in its juices, which undergo fermentation processes with ease and are transformed to biofuel (WANG et al. 2013). Research published by REN et al. (2013) showed that plantation of this plant are more profitable then cotton and corn considering lower energy intake and higher energy production yield.

Giant miscanthus (*Miscanthus giganteus*)

It is a high multiyear grass, with stems similar to reed (KLUDZE et al 2012). Within a yearly time of plantation the plant grows 3.5 meters high. It is harvested from January to March. It resistant to low temperatures with maintenance of high CO_2 assimilation and harvest yield (COPELAND et al. 2012). It harvest is 20 to 26 tons from hectare of space during the year (PARK et al. 2012). Miscanthus production cycle is 15 years (VENTURI et al. 1999). The plant aside from energy purposes can be used for reclamation industrially degraded territories (HOWANIEC, SMOLIŃSKI 2011). Miscanthus is interesting as energy dedicated crop because of its ability to decrease of anthropogenic CO_2. It is caused by the fact that the amount of CO_2 which is brought to the atmosphere during biomass burning will not exceed the amount that was accumulated by the plant during photosynthesis. It needs very few nutrients, thus can be grown on low nutrient soils. High resistance to varmints allows planting without the need of pesticide use (ANGELINI 2009). Miscanthus can be used for burning for heat production, for cellulose production, and for furniture production as isolation material (ACAROGLU, AKSOY 2005).

Jerusalem artichokes (*Helianthus tuberosus*)

It is a multiyear bulbous plant of high energetic potential. It characterized by quick growth and plantations do not require large amounts of fertilizers, pesticides or water. It can be planted on soils of low agricultural usefulness. Its energy production use is based on biofuel production, mainly bioethanol (LU et al. 2011). Harvest is between 60 to 90 tons of fresh mass per hectare. Bulbous of Jerusalem artichokes contain about 80% water, 15% carbohydrates, 1–2% protein and small amount of fat. The main sugar of this plant is insulin, and in smaller amounts saccharose, glucoses and fructose (MATIAS et al. 2011).

Oil palm (*Elaeis guineensis*)

This plant is no as common in Europe as those mentioned above, but is highly popular in Asia (exp Malaysia). It is a south African plant. It is used for production of edible oil from its fruits. The exploitation of the palm begins 3 years after its planting to 12–13 years maximum. In later periods the harvest decreases to 25^{th} year. Oil palms can be grown in all tropical countries, thus their availability for biomass production increases. Biomass of oil palm is mostly cellulose, hemicelluloses and lignin (KELLY-YONG et al. 2007, MOHAM-

MED et al. 2011). The palm fruit contains of a seed surrounded by oily mass. Oil is obtained in extraction process from cellulose mass of the fruit. Such oil can be used for edible purposes, but seed oil is used for soap production (SHUIT et al. 2009).

Agricultural wastes

In the process of agricultural production a lot of unused biomass is obtained. Agricultural wastes can be divided according to agriculture branches of their origin. Four basic groups can be outlined: wastes from field plantations, waste from food processing, breeding and slaughter wastes. It consists mainly of: manure, slurry, post slaughtering sediments leftovers from fruit and vegetables, straw, stems, whey, molasses, dairy production waste and others (CURKOWSKI et al. 2011). The problems with economically beneficial energy production from agricultural wastes is their high accumulation costs, and costs of transport from obtainment spot to utilization and storage point (DODIĆ et al. 2010).

Agricultural biomass can be used in industry for direct burning, for vaporization and fermentation. Vaporization process is very beneficial because of gas and liquid fuels shortage, and as means of heat production (DODIĆ et al. 2010). Utilization of agricultural biomass is possible not only in temperate climate but also in warmer countries. Malaysia is one of the largest producers of palm oil, which causes the need of production waste utilization. Waste are processed to animal fodder or fertilizer, but research are being done on biofuels utilization (bioethanol) and their processing to electric energy (SHUIT et al. 2009).

Wastes of food and agriculture industry

Rapidly developing food and agriculture industry generates large amounts of waste (peelings, seeds, mill cakes of juice and beer production, distillery stillage, whey, mushroom substrates, fish waste, slaughter waste and others) which are useful for renewable energy production (OLGUIN et al. 1995). This problem is the source of interest for Chair of Foundations of Safety from University of Warmia and Mazury in Olsztyn. At the moment the research on utilization of post beet pulp fermentation wastes from methane production are being conducted. In the last few years beet pulp from a desirable resource have become a troublesome waste. Work on utilizing them as fertilizers for energy dedicated willow are in progress.

Methane fermentation and biogas

Fermentation is a process of organic matter degradation by microorganisms in non oxygen environment. One of the fermentation products is biogas, which consists mainly of methane and carbon dioxide. In order to increase the production yield multisubstrate fermentation can be conducted (WU 2007). Fermentation processes are often utilized for stabilization of liquid and solid waste (LUSTRATO et al. 2012). Biogas production from agricultural wastes, animal excrements and municipal and industrial wastes is a potential alternative energy source for many countries. One cubic meter of biogas can produce 2.1 kWh electric and 2.9 kWh heat energy equivalent (ZIEMIŃSKI, FRĄC 2012). In 20th century 90's multiple benefits of biogas have been observed, as well as multitude of biomass sources, which could have been utilized for production of this resource (GUNASEELAN 1997). Such production is also one of utilization methods for food industry wastes, such as sugar wastewater (OLGUIN et al. 1995). Biogas is not only methane and CO_2, but also hydrogen. Hydrogen is more and more often described as the fuel of the future, and methods of its production are subject of many research. One of the sources of bio-hydrogen, considering its high concentration with relatively low nitrogen rate, are sugar industry and cellulose production wastes, as well as other wastes of high carbohydrates concentration. The wastes from plant watering are also worth consideration. Plants decrease the amounts of nitrogen, but wastes are still a rich hydrogen source (KAPDAN, KARGI 2006). A interesting solution is production of hydrogen from fermentation wastewater. Process is a two step fermentation, which leads to production of hydrogen in the first phase and production of methane in second phase. As substrate some of the algae like *Laminaria japonica* (JUNG et al. 2012) can be utilized, but also, what is more important from recycling point of view, food industry wastes (KIM et al. 2012).

Conclusions

With growing industrial development the need for energy increases. However because of growing environmental awareness in the society emphasis is being put on acquiring more amounts of energy from renewable resources then from not renewable ones. Biomass is an example of such energy sources. In light of presented studies a large variety of biomass and potential for its application for energy production purposes. It is possible to select energy dedicated crop for given climate and soil type as well as proper waste utilization. Considering this energy sources obtained during food – agricultural production processes are perspective for clean energy production. Because of Poland geographical location and need for energy sources diversification

biomass energy seems to be especially beneficial for north-east regions of Poland.

References

ACAROGLU M., AKSOY A.S. 2005. *The cultivation and energy balance of Miscanthus x giganteus production in Turkey.* Biomass and Bioenergy, 29: 42–48.

ANGELINI L.G., CECCARINI L., NASSI O DI NASSO N., BONARI E. 2009. *Comparison of Arundo donax L. and Miscanthus x giganteus in a long term field experiment in Central Italy: Analysis of productive characteristics and energy balance.* Biomass and Bioenergy, 33: 635–643.

BANOS R., MANZANO-AGUGLIARO F., MONTOYA F.G., GIL C., ALCAYDE A., GÓMEZ J. 2011. *Optimization methods applied to renewable and sustainable energy: A review*. Renewable and Sustainable Energy Reviews, 15: 1753–1766.

COPELAND N., CAPE J.N., HEAL M.R. 2012. *Volatile organic compound emissions from Miscanthus and short rotation coppice willow bioenergy crops.* Atmospheric Environment, 60: 327–335.

CURKOWSKI A., ONISZK-POPŁAWSKA A., MROCZKOWSKI P., ZOWSIK M., WIŚNIEWSKI G. 2011. *Przewodnik dla inwestorów zainteresowanych budową biogazowni rolniczych*. Instytut Energii Odnawialnej, Warszawa.

DEMIRBAS A. 2008. *Importance of biomass energy sources for Turkey*. Energy Policy, 36: 834–842.

DODIĆ S.N., ZEKIĆ V.N., RODIĆ V.O., TICA N.L., DODIĆ J.M., POPOV S.D. 2010. *Situation and perspectives of waste biomass application as an energy source in Serbia.* Renewable and Sustainable Energy Reviews, 14: 3171–3177.

DODIĆ S.N., ZELENOVIĆ VASILJEVIĆ T., MARIĆ R.M., KOSANOVIĆ A.J.R., DODIĆ J.M., POPOV S.D. 2012. *Possibilities of application of waste wood biomass as an energy source in Vojvodina.* Renewable and Sustainable Energy Reviews, 16: 2355–2360.

Energy from renewable sources 2011. 2012. GUS, Warsaw, on line: http://www.stat.gov.pl/gus/5840_3680_PLK_HTML.htm (available: 15.12.2012).

FILLION M., BRISSON J., TEODORESCU T.I., SAUVE S., LABRECQUE M. 2009. *Performance of Salix viminalis and Populus nigra x Populus maximowiczii in short rotation intensive culture under high irrigation.* Biomass and Bioenergy, 33: 1271–1277.

GUNASEELAN V.N. 1997. *Anaerobic digestion of biomass for methane production: a review*. Biomass and Bioenergy, 13(1/2): 83–114.

HOWANIEC N., SMOLIŃSKI A. 2011. *Steam gasification of energy crops of high cultivation potential in Poland to hydrogen-rich gas*. International Journal of Hydrogen Energy, 36: 2038–2043.

JAMA A., NOWAK W. 2012. *Willow (Salix viminalis L.) in purifying sewage sludge treated soils.* Polish Journal of Agronomy, 9: 3–6.

JUNG K.W., KIM D.H., SHIN H.S. 2012. *Continuous fermentative hydrogen and methane production from Laminaria japonica using a two-stage fermentation system with recycling of methane fermented effluent.* International Journal of Hydrogen Energy, 37: 15648–15657.

KAPDAN I.K., KARGI F. 2006. *Bio-hydrogen production from waste materials*. Enzyme and Microbial Technology, 38: 569–582.

KELLY-YONG T.L., LEE K.T., MOHAMED A.R., BHATIA S. 2007. *Potential of hydrogen from oil palm biomass as a source of renewable energy worldwide.* Energy Policy, 35: 5692–5701.

KIM S.H. CHEON H.C., LEE C.Y. 2012. *Enhancement of hydrogen production by recycling of methanogenic effluent in two-phase fermentation of food waste*. International Journal of Hydrogen Energy, 37: 13777–13782.

KLUDZE H., DEEN B., DUTTA A. 2012. *Impact of agronomic treatments on fuel characteristics of herbaceous biomass for combustion.* Fuel Processing Technology, on line: http://ac.els-cdn.com/S0378382012003694/1-s2.0-S0378382012003694-main.pdf?_tid=a316d14e-58c1-11e2-82a7-00000aab0f6b acdnat=1357560126–7438d4a82859fd0f3bc9509cd2678a0a (accessible 27.12.2012).

LIM J.S., MANAN Z.A., ALWI S.R.W., HASHIM H. 2012. *A review on utilization of biomass from rice industry as a source of renewable energy.* Renewable and Sustainable Energy Reviews, 16: 3084–3094.

Liu Z.X., Han L.P., Steinberger Y., Xie G.H. 2011. *Genetic variation and yield performance of Jerusalem artichoke germplasm collected in China.* Agricultural Sciences in China, 10(5): 668–678.

Lustrato G., Alfano G., Ranalli G. 2012. *Bio-hydrogen and bio-methane co-production by sequential two-phases dark fermentation from agro-industrial wastes (IMERA).* Environmental Engineering and Management Journal, 11(3–Suplement): S76.

Mant C., Peterkin J., May E., Butler J. 2003. *A feasibility study of Salix viminalis gravel hydroponic system to renovate primary settled wastewater*. Bioresource Technology, 90: 19–25.

Marmiroli M., Robinson B.H., Clothier B.E., Bolan N.S., Marmiroli N., Schulin R. 2012. *Effect of dairy effluent on the biomass, transpiration, and elemental composition of Salix kinuyanagi Kimura.* Biomass and Bioenergy, 37: 282–288.

Matias J., Gonzales J., Royano L., Barrena L.A. 2011. *Analysis of sugars by liquid chromatography-mass spectrometry in Jerusalem artichoke tubers for bioethanol production optimization.* Biomass and Bioenergy, 35: 2006–2012.

Matsakas L., Christakopoulos P. 2013. *Fermentation of liquefacted hydrothermally pretreated sweet sorghum bagasse to ethanol at high-solids content*. Bioresource Technology, 127: 202–208.

Meki M.N., Snider J.L., Kiniry J.R., Raper R.L., Rocateli A.C. 2013. *Energy sorghum biomass harvest thresholds and tillage effects on soil organic carbon and bulk density.* Industrial Crops and Products, 43: 172–182.

Mohammed M.A.A., Salmiaton A., Wan Azlina W.A.K.G., Mohammad Amran A.S., Fakhru'l-Razi A., Taufiq-Yap Y.H. 2011. *Hydrogen rich gas from oil palm biomass as a potential source of renewable energy in Malaysia.* Renewable and Sustainable Energy Reviews, 15: 1258–1270.

Olguin E.J., Doelle H.W., Mercado G. 1995. *Resource recovery through recycling of sugar processing by-products and residuals.* Resources Conservation and Recycling, 15: 85–94.

Park H.J., Park K.H., Jeon J.K., Kim J., Ryoo R., Jeong K.E., Park S.H., Park Y.K. 2012. *Production of phenolics and aromatics by pyrolysis of miscanthus.* Fuel, 97: 379–384.

Ren L.T., Liu Z.X., Wei T.Y., Xie G.H. 2012. *Evaluation of energy input and output of sweet sorghum grown as a bioenergy crop on coastal saline-alkali land*. Energy, 47: 166–173.

Sayigh A. 2012. *Renewable energy: The only solution*. International Journal of Environment and Sustainability, 1(3): 83–86.

Shuit S.H., Tan K.T., Lee K.T., Kamaruddin A.H. 2009. *Oil palm biomass as a sustainable energy source: A Malaysian case study*. Energy, 34: 1225–1235.

Stolarski M. 2003. *Wszystko o wierzbie*. Czysta Energia, 25(10): 32–33.

Suntana A.S., Vogt K.A., Turnblom E.C., Upadhye R. 2009. *Bio-methanol potential in Indonesia: Forest biomass as a source of bio-energy that reduces carbon emissions*. Applied Energy, 86: 215–221.

Tahvanainen L., Rytkonen V.M. 1999. *Biomass production of* Salix viminalis *in southern Finland and the effect of soil properties and climate conditions on its production and survival*. Biomass and Bioenergy, 16: 103–117.

Venturi P., Gigler J.K., Huisman W. 1999. *Economical and technical comparison between herbaceous (Miscanthus x giganteus) and woody energy crops (Salix viminalis).* Renewable Energy, 16: 1023–1026.

Wang L., Luo Z., Shahbazi A. 2013. *Optimization of simultaneous saccharification and fermentation for the production of ethanol from sweet sorghum (Sorghum bicolor) bagasse using response surface methodology.* Industrial Crops and Products, 42: 280–291.

Wu W. 2007. *Anaerobic co-digestion of biomass for methane production*: *recent research achievements*. Iowa State University. On line: home.eng.iastate.edu/~tge/ce421-521/wei.pdf (available: 6.12.2012).

Zagorskis A., Baltrenas P., Misevicius A., Baltrenaite E. 2012. *Biogas production by anaerobic treatment of waste mixture consisting of cattle manure and vegetable remains*. Environmental Engineering and Management Journal, 4: 849–856.

Ziemiński K., Frąc M. 2012. *Methane fermentation process as an anaerobic digestion of biomass: Transformations, stages and microorganisms*. African Journal of Biotechnology, 11(18): 4127–4139.

Technical Sciences 16(3), 2013, 221–231

EFFECTS OF NONLINEARITY ON BOLT FORCES FOR THE OPERATIONAL STATE OF A MULTI-BOLTED CONNECTION

Rafał Grzejda

Department of Mechanics and Fundamentals of Machine Design
West Pomeranian University of Technology in Szczecin

Received 29 July 2013; accepted 10 September 2013; available on line 27 September 2013

K e y w o r d s: multi-bolted connection, operational state, bolt force.

A b s t r a c t

In the paper modelling and calculations of an asymmetrical multi-bolted connection at the operational stage are presented. The physical model of the joint is based on a flexible flange element that is connected with a rigid support by means of linear spring elements, which substitute bolts. Between the flange element and the support, the linear Winkler model of a contact layer is taken into consideration. The multi-bolted system is preloaded and then subjected to an eccentric normal load. Influence of nonlinearity of the contact layer between joined elements on computational values of bolt forces has been investigated. Results of calculations for several different values of the joined element's thickness are pointed out.

Introduction

Multi-bolted connections are systems of many contacting bodies. Characteristics of contact joints are usually nonlinear. Accordingly, multi-bolted connections should be treated as the nonlinear systems. The source of this nonlinearity are also gaskets and washers, which are often used in such joints (BOUZID, CHAMPLIAUD 2003, SAWA et al. 2003). However, the extent of this nonlinearity depends on loads acting on the connection. It can be made an argument that for analyses of a multi-bolted connection at the operational

Corespondence: Rafał Grzejda, Katedra Mechaniki i Podstaw Konstrukcji Maszyn, Zachodniopomorski Uniwersytet Technologiczny, ul. Piastów 19, 70-310 Szczecin, phone: +48 91 449 49 69, fax: +48 91 449 45 64, e-mail: rafal.grzejda@zut.edu.pl.

stage, the assumption of nonlinearity of the contact layer between joined elements is not recommended. This is possible under the following conditions:
– the multi-bolted connection is preloaded,
– characteristics of the nonlinear contact layer are described as a power function (MISRA, HUANG 2012, WANG et al. 2013) or a polynomial function (KONOWALSKI 2009, YASTREBOV et al. 2011).

In the previous paper (WITEK, GRZEJDA 2005) some results of theoretical investigations of an asymmetrical preloaded multi-bolted connection of a flange and a rigid support, subjected to an external normal load, were released. In the model of the joint, bolts were treated as linear springs and between the flange element and the support, the nonlinear model of the contact layer was taken into consideration. In the current paper some new results of investigations of an analogical model of the joint are presented. In the new model, the linear model of the contact layer between joined elements is taken into account. For modelling and calculations of the multi-bolted connection the finite element method – FEM (ZIENKIEWICZ, TAYLOR 2005) is used.

Physical model of the multi-bolted connection

A general structure of the multi-bolted connection model results from an idea presented in article (WITEK, GRZEJDA 2005). The model of the joint is based on a flexible flange element that is fastened to a rigid support by means of k one-sided linear spring elements (GRZEJDA 2009), which substitute bolts, preloaded by forces F_{mi} (Fig. 1*b*). Spring properties of the i-th bolt's model (for $i = 1, 2, ..., k$) are determined from the formula

$$c_{yi} = \frac{1}{\sum_n \frac{1}{c_n}} \tag{1}$$

where:
c_n – denotes the linear stiffness coefficient of the n-th bolt's fragment.

A contact layer between the flange element and the support is modeled as the Winkler model (WANG et al. 2005). This type of the contact layer may be applied in this case, because the considered joint is loaded only by normal forces. The Winkler model of the contact layer is described by means of l one-sided linear spring elements, which are discretely distributed in the contact plane and characterized by the following relationship

$$R_j = A_j \cdot \mathrm{f}(u_j) \tag{2}$$

where:
R_j – the force in the centre of the j-th elementary contact area,
A_j – the j-th elementary contact area,
u_j – deformation of the j-th linear spring element (for $j = 1, 2, ..., l$).

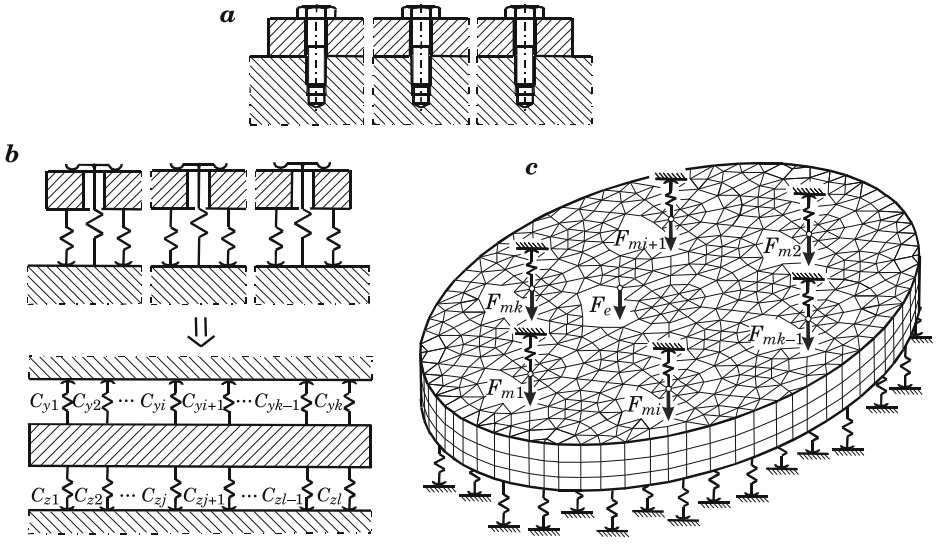

Fig. 1. Multi-bolted connection: *a* – diagram of the joint, *b* – description of system spring properties, *c* – FEM-model of the joint (composed of linear springs, which substitute bolts; the discrete flange element and linear springs, which are elements of the contact layer)

Creation of the finite element mesh at the contact surface of joined elements consists in performing the following steps:

– division of the contact area between joined elements into elementary contact areas,

– determination of the centres of gravity of individual elementary contact areas,

– insertion nodes at the centres of gravity of elementary contact areas,

– addition linear spring elements at the nodes defined in the previous phase.

The equation of system equilibrium (Fig. 1) can be written as

$$\mathbf{K} \cdot \boldsymbol{q} = \mathbf{p} \tag{3}$$

where:
$\mathbf{K}$ – the stiffness matrix,
$\boldsymbol{q}$ – the displacements vector,
$\boldsymbol{p}$ – the loads vector.

In the operational state, the loads vector $\boldsymbol{p}$ is composed of external normal loads F_e (Fig. 1*c*).

The generating procedure of the stiffness matrix $\mathbf{K}$ is presented in works (GRZEJDA 2009, WITEK, GRZEJDA 2005). Adopting the division of the joint into three subsystems (B – the set of bolts, F – the flange element model, C – the linear Winkler model of the contact layer), (3) can be rewritten in the form

$$\begin{bmatrix} \mathbf{K}_{BB} & \mathbf{K}_{BF} & \mathbf{0} \\ \mathbf{K}_{FB} & \mathbf{K}_{FF} & \mathbf{K}_{FC} \\ \mathbf{0} & \mathbf{K}_{CF} & \mathbf{K}_{CC} \end{bmatrix} \cdot \begin{bmatrix} \boldsymbol{q}_B \\ \boldsymbol{q}_F \\ \boldsymbol{q}_C \end{bmatrix} = \boldsymbol{p} \tag{4}$$

where:
$\mathbf{K}_{BB}$, $\mathbf{K}_{FF}$ $\mathbf{K}_{CC}$ – are the stiffness matrices of subsystems B, F, C,
$\mathbf{K}_{BF}$, $\mathbf{K}_{FB}$, $\mathbf{K}_{FC}$, $\mathbf{K}_{CF}$ – are the matrices of elastic couplings among subsystems B, F, C.

On the grounds of so defined model of the multi-bolted connection, displacements of bolts and bolt forces after the operational state has been completed can be evaluated.

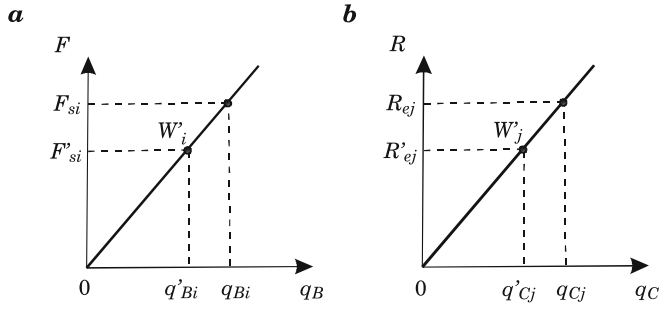

Fig. 2. Determining of the working load: *a* – in the case of linear springs, which substitute bolts, *b* – in the case of linear springs, which are elements of the contact layer

A starting point for calculations of the multi-bolted connection at the operational stage are the data obtained at the end of its assembly operation (GRZEJDA 2013, WITEK, GRZEJDA 2006). The model of the system proposed for the assembly condition makes it possible to analyze how the tightening sequence affects the preload distribution both during the multi-bolted connection's assembly and after it has been completed.

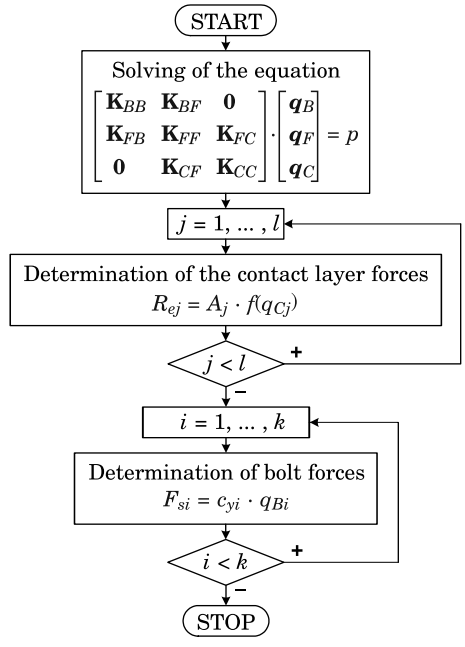

Fig. 3. Block diagram of iterative calculations of the multi-bolted connection

As a result of solving the equation (4) one obtains the displacements vector of bolts $\boldsymbol{q}_B$

$$\boldsymbol{q}_B = \text{col}(q_{B1}, q_{B2}, \ldots, q_{Bi}, \ldots, q_{Bk}) \tag{5}$$

Final displacements of bolts q_{Bi} are measured from the working points W_i', which determine tension of bolts in the previous step of calculations (Fig. 2*a*). On the basis of so defined displacements q_{Bi}, forces in bolts F_{si} can be computed using the formula

$$F_{si} = c_{yi} \cdot q_{Bi} \tag{6}$$

As a result of solving the equation (4) one obtains the displacements vector of linear springs $\boldsymbol{q}_C$ too, which can be evaluated from the relation

$$\boldsymbol{q}_C = \text{col}(q_{C1}, q_{C2}, \ldots, q_{Cj}, \ldots, q_{Cl}) \tag{7}$$

Final displacements of elements of the contact layer q_{Cj} are measured from the working points W_j', which determine their tension in the previous step of

calculations (Fig. 2*b*). On the basis of so defined displacements q_{Cj}, forces in the contact layer R_{ej} can be computed from the relation (2) for u_j equal to q_{Cj}.

The diagram of iterative calculations of the multi-bolted connection is shown in Figure 3.

Calculations of the multi-bolted connection at the operational stage

According to the presented method, computations of an asymmetrical multi-bolted connection were performed. A simplified FEM-based model of the joined element is shown in Figure 4*a*. A contact surface between joined elements as well as the bolt's arrangement and their numeration are shown in Figure 4*b*.

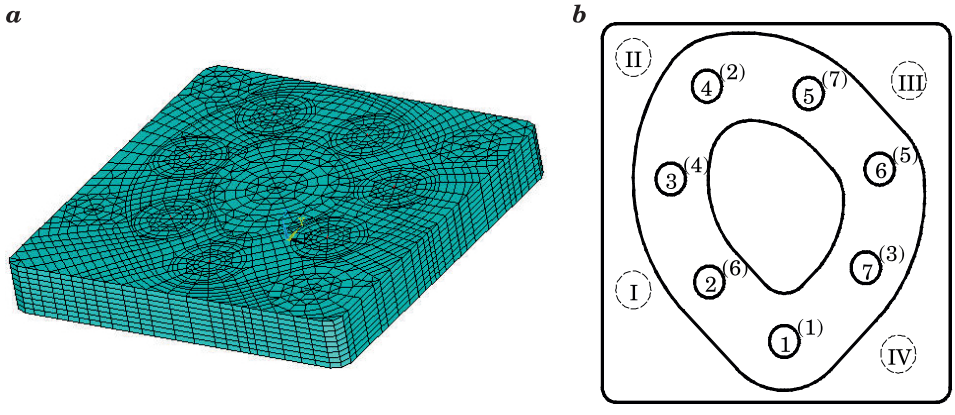

Fig. 4. Considered multi-bolted connection: *a* – simplified FEM-based model, *b* – joint characteristic

Calculations were carried out for three values of the joined element's thickness h (for $h \in \{20\text{ mm}, 40\text{ mm}, 80\text{ mm}\}$). Characteristics of linear contact springs are described as the following function (GRZEJDA 2009)

$$R_j = A_j \cdot (26.873 \cdot u_j) \tag{8}$$

To fastening of the joint, the bolts M10×1.25 were used. The standard preload of bolts F_{mi} is equal to 20 kN. The tightening sequence taken here on (GRZEJDA 2009), is parenthesized in Figure 4*b*. After the preloading process, the multi-bolted connection is subjected to an eccentric normal load F_e equal to 50 kN acting consecutively at four points (I, II, III, IV) shown in Figure 4*b*.

Calculations were realized in ANSYS software. To build the model of the multi-bolted connection, the following finite elements were applied:

– link elements, which substitute bolts,

– solid elements, to model the flange element,

– link elements with characteristics consistent with the formula (8), to model the contact layer.

The number of elements used for modelling of the multi-bolted connection as a function of the joined element's thickness is set up in Table 1.

Table 1

Size of the FEM-models as a function of the joined element's thickness

Subsystem	Number of elements		
	h = 20 mm	h = 40 mm	h = 80 mm
B	7	7	7
F	19,256	39,396	39,396
C	664	664	664

Results of calculations were put together in graphs illustrated in Figure 5 and Figure 6 according as both the individual thickness of the flange element h and four points of the load F_e acting. In the respective figures, values of bolt forces F_{si} related to preloads F_{mi} (WITEK, GRZEJDA 2006) are presented. For describing the results of calculations a following nomenclature is introduced:

– the L-model – the model of the joint with the linear Winkler model of the contact layer,

– the NL-model – the model of the joint with the nonlinear Winkler model of the contact layer (WITEK, GRZEJDA 2005).

The shape of the figures is nearly symmetrical around the points of the load F_e acting. This symmetry is determined by the nature of the adopted type of the contact layer, which takes into account only properties of the contact in the normal direction. Significant increases in the bolt forces in bolts lying closest to the points of external loading are related to high values of local contact pressure in this part of the joint.

In most of the cases, values of forces in individual bolts computed according to the L-model of the joint are smaller than their values obtained according to the NL-model of the joint. Analysis of relative difference between obtained bolts forces is done on the basis of the W index

$$W = \left| \frac{F^{L}_{s\,\max} - F^{NL}_{s\,\max}}{F^{NL}_{s\,\max}} \right| \tag{9}$$

where:
$F^{L}_{s\,\max}$ – the maximal force in the bolt according to the L-model of the joint,
$F^{NL}_{s\,\max}$ – the maximal force in the bolt according to the NL-model of the joint.

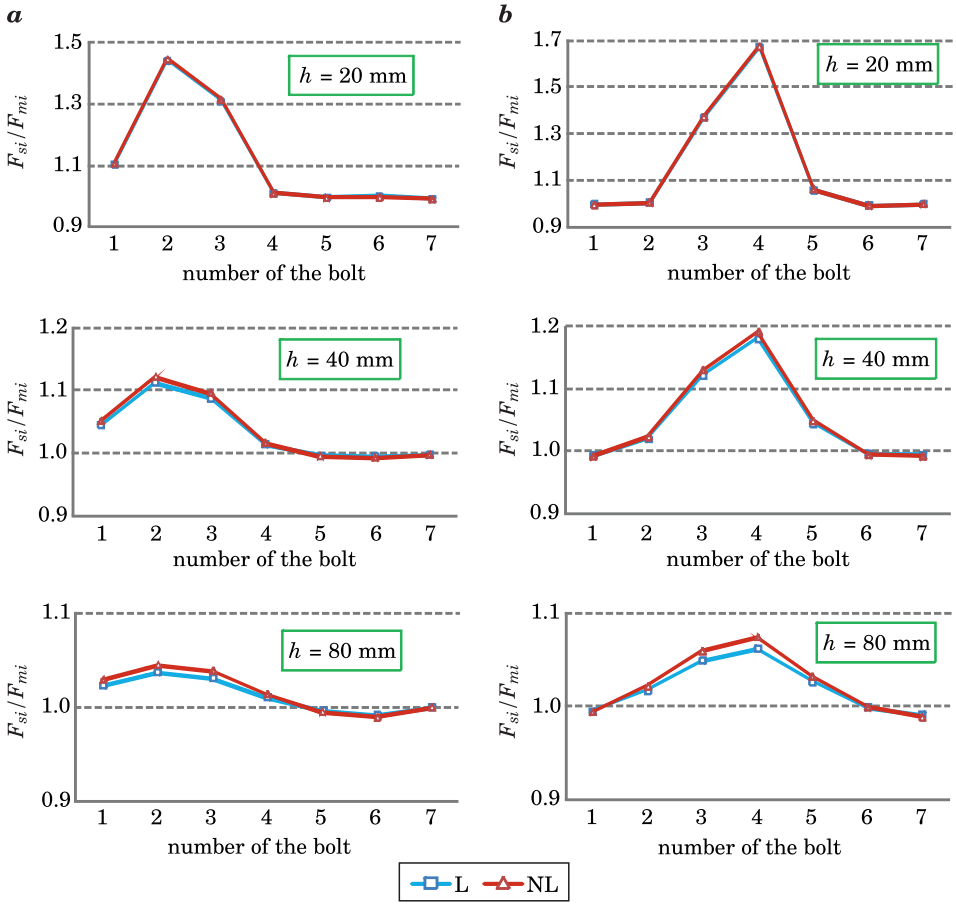

Fig. 5. Bolt load values in the joint externally loaded at the point: *a* – I, *b* – II

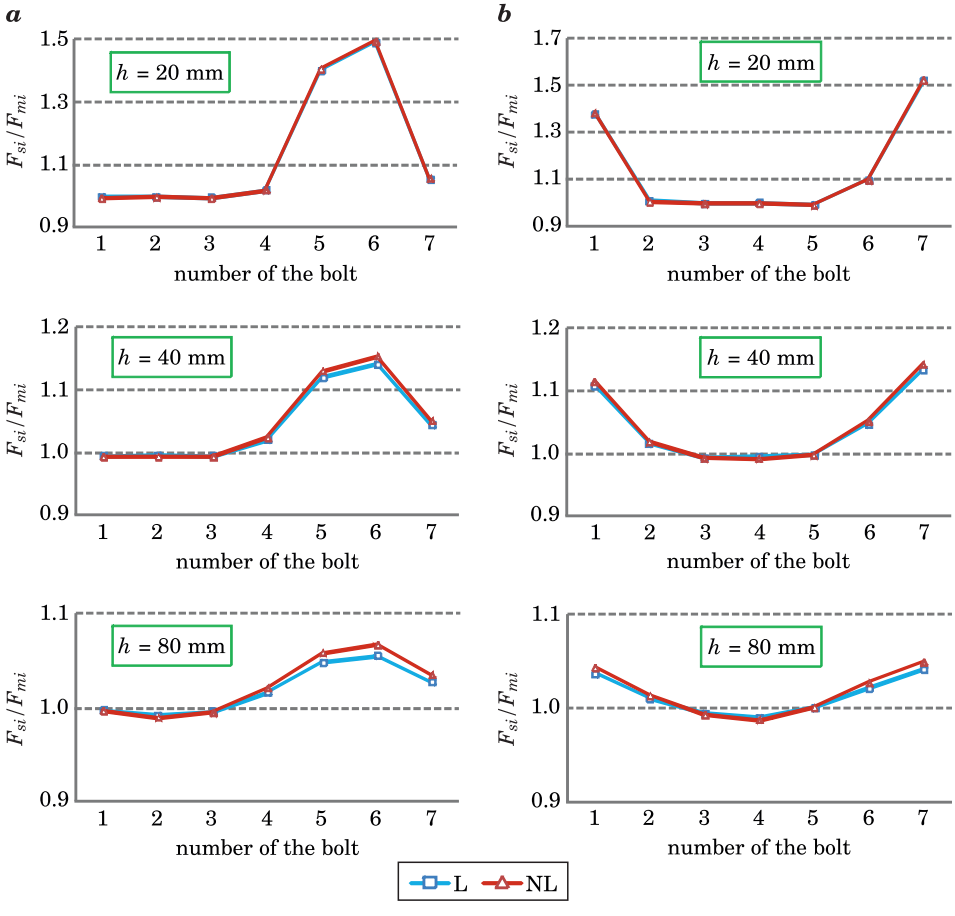

Fig. 6. Bolt load values in the joint externally loaded at the point: *a* – III, *b* – IV

Table 2

W index values as a function of the joined element's thickness

	h = 20 mm	h = 40 mm	h = 80 mm
W [%]	Point No. I		
	0.41	0.81	0.78
	Point No. II		
	0.28	0.87	1.10
	Point No. III		
	0.36	1.05	1.12
	Point No. IV		
	0.34	0.68	0.75

W index values as a function of the thickness of the joined element are set up in Table 2. On the grounds of comparisons, it can be noted that the accuracy of calculations results by means of the linear multi-bolted connection model decreases with reduction of joined element's flexibility. Depending on the joined element's thickness, the error of estimation may range from 0.28 to 1.12%.

Conclusions

In the case of multi-bolted connections preloaded pursuant to technical standards and then subjected to an eccentric normal load, nonlinearity of the contact layer between joined elements has negligible influence on computational values of bolt forces. Wherefore for analyses of such joints, the linear Winkler model of the contact layer can be applied. Owing to this fact, one achieves significantly higher efficiency of the modelling, which is brought on both the smaller complexity of the problem and considerably shorter process time.

The block construction of the multi-bolted connection model allows to expand its applicability. This is possible by modifying individual subsystems *B*, *F* or *C*. In the case of using this model to analyses of the joint loaded by an arbitrary force, it would be necessary to apply a different type of the contact layer model.

The presented model of the multi-bolted connection can be successfully used also in load capacity analysis of any joint in which a flexible flange element is connected with a rigid support (for a review, see DOMINIKOWSKI, BOGACZ 2009).

References

BOUZID A.H., CHAMPLIAUD H. 2003. *On the use of dual kriging interpolation for the evaluation of the gasket stress distribution in bolted joints*. Analysis of bolted joints, Proc. of the 2003 ASME Pressure Vessels and Piping Conference, Cleveland, Ohio, p. 77–83.

DOMINIKOWSKI S., BOGACZ P. 2009. *Determination of internal forces in end plates of simple end plate joints*. Technical Sciences, 12: 83–94.

GRZEJDA R. 2009. *Modelling and analysis of a multi-bolted joint of a flange element fastened to a nonlinear spring layer*. Doctor's thesis, West Pomeranian University of Technology, Szczecin.

GRZEJDA R. 2013. *Effects of nonlinearity of a contact layer between elements joined in a multi-bolted connection on preload values in bolts*. Bulletin of the Military University of Technology, article in press.

KONOWALSKI K. 2009. *Experimental research and modeling of normal contact stiffness and contact damping of machined joint surfaces*. Advances in Manufacturing Science and Technology, 33(3): 53–68.

MISRA A., HUANG S. 2012. *Micromechanical stress-displacement model for rough interfaces: Effect of asperity contact orientation on closure and shear behavior*. International Journal of Solids and Structures, 49(1): 111–120.

SAWA T., IWAMOTO T., FUNADA K., OMIYA Y. 2003. *FEM stress analysis and sealing performance in pipe flange connections with gaskets subjected to external bending moment (case where internal fluid is liquid)*. Analysis of bolted joints, Proc. of the 2003 ASME Pressure Vessels and Piping Conference, Cleveland, Ohio, p. 85–95.

WANG L., LIU H., ZHANG J., ZHAO W. 2013. *Analysis and modeling for flexible joint interfaces under micro and macro scale*. Precision Engineering, 37(4): 817–824.

WANG Y.H., THAM L.G., CHEUNG Y.K. 2005. *Beams and plates on elastic foundations: a review*. Progress in Structural Engineering and Materials, 7(4): 174–182.

WITEK A., GRZEJDA R. 2005. *Analysis of a nonlinear multi-bolted joint loaded by a normal force*. Archives of Mechanical Technology and Automation, 25(2): 211–219.

WITEK A., GRZEJDA R. 2006. *An analysis of the preload of a nonlinear multi-bolted joint*. Archives of Mechanical Technology and Automation, 26(2): 271–280.

YASTREBOV V.A., DURAND J., PROUDHON H., CAILLETAUD G. 2011. *Rough surface contact analysis by means of the Finite Element Method and of a new reduced model*. Comptes Rendus Mécanique, 339(7–8): 473–490.

ZIENKIEWICZ O.C., TAYLOR R.L. 2005. *The finite element method for solid and structural mechanics*. Elsevier Butterworth-Heinemann, Oxford.

Technical Sciences 16(3), 2013, 234–247

A THEORETICAL ANALYSIS OF CEREAL SEED SCREENING IN A STRING SIEVE

Zdzisław Kaliniewicz

Department of Heavy Duty Machines and Research Methodology
University of Warmia and Mazury, Poland

Received 22 June 2013, accepted: 23 October 2013, available on line 23 October 2013

K e y w o r d s: string sieve, modelling, seeds, angle of inclination.

A b s t r a c t

The conditions of the screening process in a fixed string sieve designed by the author have been formulated. The string sieve was designed for separating seeds of 5 cereal species (wheat, rye, barley, oats and triticale). The width of the separating groove was set at 1 mm at the beginning of the screen and 5 mm at the end of the screen. It has been assumed that seeds have a spheroidal shape and that their motion is initiated by positioning the string sieve at an appropriate angle. The results of a theoretical analysis revealed that at the given parameters of a string sieve, the above angle is determined only by the thickness and width of separated seeds. The sieve's angle of inclination should be set at 45° to propel seeds into motion and at 50° to ensure the continuity of the screening process. Such a large setting angle is not recommended because it increases the sieve's height and deteriorates the quality of the separation process. The problem can be solved by setting the separator bucket into motion and separating seeds at a small inclination angle of the string sieve.

Symbols:
a, b – seeds thickness and width, mm,
d – equivalent diameter of seed width and thickness, mm
D_s – string diameter, mm,
e – distance from the beginning of the screen, mm,
g – gravitational acceleration, $m \cdot s^{-2}$,
G, G_y, G_{y1}, G_{y2}, G_z – gravity force and gravity force components, N,
L_s – screen length, mm,
m – seed weight, kg,
N_1, N_2, N_{1x}, N_{1z}, N_{2x} – the string's normal ground reaction forces and normal ground reaction force components, N,
R_s – string spacing, mm,
s – width of groove at distance a from the beginning of the screen, mm,
s_k – width of separating groove at the end of the screen, mm,
s_p – width of separating groove at the beginning of the screen, mm,

Corespondence: Zdzisław Kaliniewicz, Katedra Maszyn Roboczych i Metodologii Badań, Uniwersytet Warmińsko-Mazurski, ul. Oczapowskiego 11/B112, 10-719 Olsztyn, phone:+ 48 89 523 39 34, e-mail: zdzislaw.kaliniewicz@uwm.edu.pl

s_1 – width of groove at distance $^3/_4$ e from the beginning of the screen, mm
T_1, T_2 – frictional force components, N,
x, SD – average value and standard deviation of trait,
x_{min}, x_{max} – minimum and maximum value of trait,
α – angle of inclination of a string sieve, °,
γ – opening angle between strings in bottom rows, °,
μ_k – coefficient of sliding friction of a cereal seed,
μ_s – coefficient of static friction of a cereal seed,
φ – included angle between the seeds' gravity force component and a string's normal ground reaction force, °.

Introduction

Seed mixtures are cleaned and sorted with the involvement of separators that rely on the aerodynamic and geometric characteristics of processed material (BERLAGE et al. 1984, CĂSĂNDROIU et al. 2009, GROCHOWICZ 1994, LI et al. 2002, RAWA 1992, RAWA et al. 1990, SIMONYAN, YILJEP 2008, VOICU, CĂSĂNDROIU 2004, WANG et al. 1994, WIERZBICKI et al. 1991). This group of separators includes string sieves which should be equipped with a set of wire and/or mesh screens with differently shaped and/or sized openings to maximize the effectiveness of the separation process. Several mesh screens appropriate for the separated mixture are selected and placed in the separator bucket. The screens available from the machine supplier generally have fixed mesh openings, which limits the separation effectiveness of seeds that belong to the same species and variety but differ in plumpness.

A string sieve is a solution that flexibly adapts to variations in the parameters of the separated seed mixture (KALINIEWICZ 2011, 2013a). Strings are stretched between two horizontal bars (Fig. 1). This arrangement creates a separating groove along the screen, and the size of the separating groove changes gradually with distance from the beginning of the screen in the range of s_p to s_k. At the beginning of the screen, the width of the openings between strings is smaller than the thickness of the finest seeds, and the openings at the end of the screen are larger than the thickness of the largest seeds of the principal species. In view of the average size of farm-produced seeds, the width of the separating groove should be set at 1 mm at the beginning of the screen and 11 mm at the end of the screen. In sieves not designed for grading large seeds or vetch seeds, the width of the separating groove can be set at 1 mm and 5 mm, respectively. Seeds are sorted into various size fractions by changing the position of collecting buckets under the screen (KALINIEWICZ 2013a).

The angle of inclination of a separator screen is also an important consideration which determines the effectiveness and continuity of the separation process.

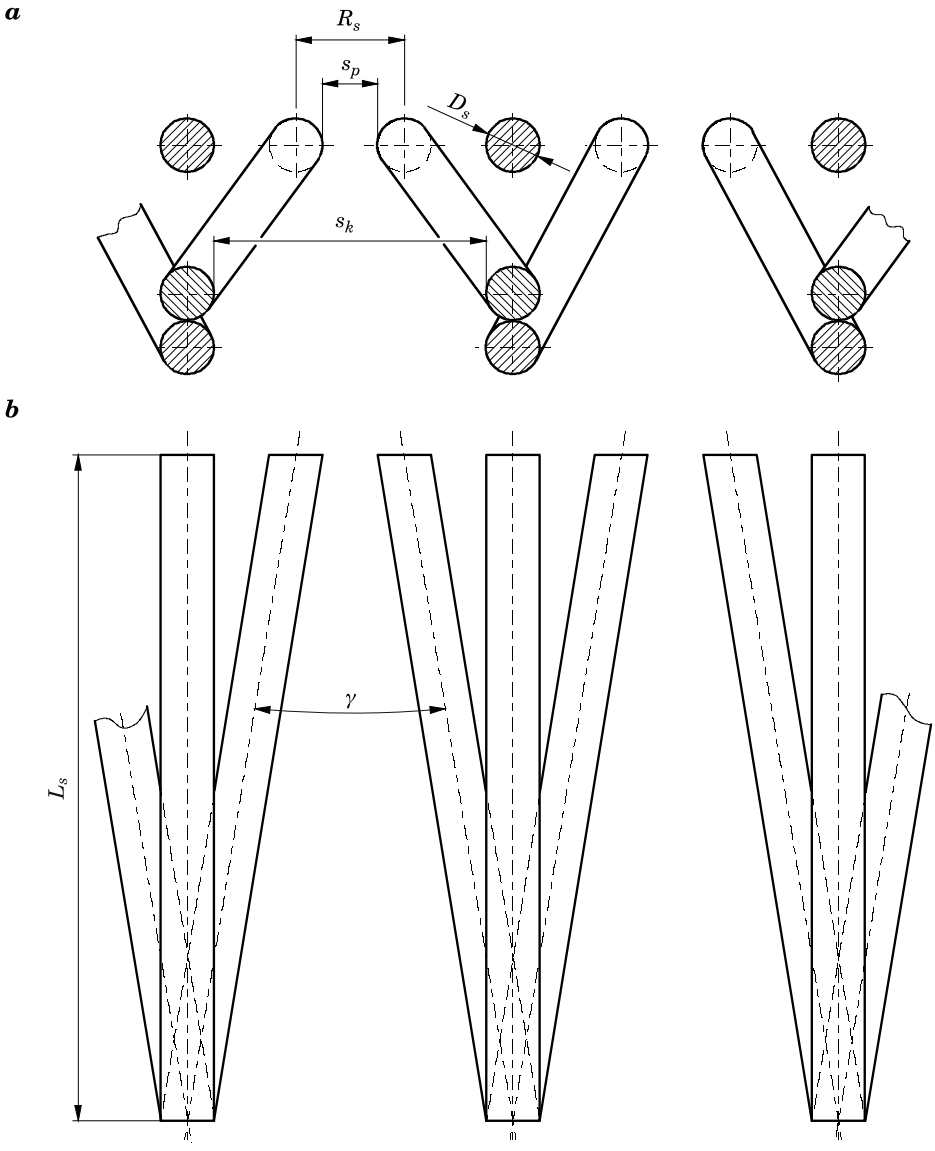

Fig. 1. String arrangement in a string sieve: *a* – rear view, *b* – top view
Source: KALINIEWICZ (2013a).

This paper analyzes the movement of grain seeds on a fixed string sieve with the aim of determining the screen's angle of inclination that guarantees maximum separation effectiveness.

Theoretical analysis

It was assumed that the string sieve is made of wires, rods or strings with circular cross-section. Strings are made of steel, and they may be additionally coated with plastic or rubber. A narrow stream of seeds is fed from the seed container to the initial section of the string sieve with the smallest width of separating grooves. The surface of the string sieve is set at angle α relative to the horizontal plane (Fig. 2). Since seeds are not fed into the sieve individually, some of them are blocked by other seeds, and their motion is initiated with a certain delay. Therefore, it was assumed that the initial velocity of seeds equals zero and that seeds are set into motion by the force of gravity. It was also assumed that the motion of each seed is self-initiated and it is not affected by other seeds. For the sake of simplicity, the following angles were disregarded: opening angle between strings in bottom rows, angle of inclination of bottom strings in the first row relative to top strings, and angle of inclination of bottom strings in the second row relative to top strings. The observed angles are small, and they do not exceed 1.5° even in the shortest screens with the widest separating grooves at the end of the screen (KALINIEWICZ 2013a).

In line with the models proposed by other authors (GASTÓN et al. 2002, GROCHOWICZ 1994, HEBDA, MICEK 2005, 2007, ZDYBEL et al. 2009, ŻABIŃSKI,

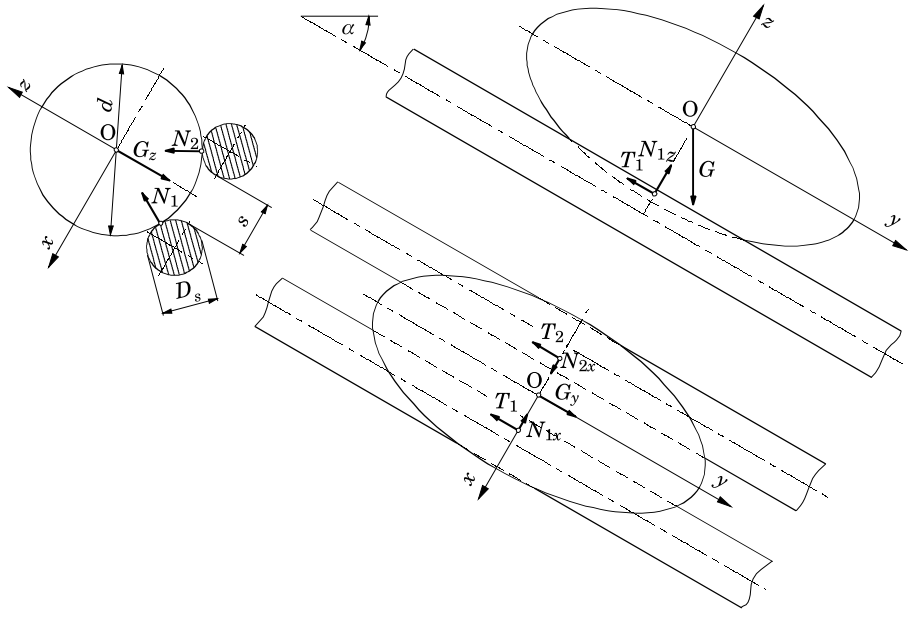

Fig. 2. Forces acting upon cereal seeds at the beginning of a string sieve

SADOWSKA 2010), the geometrical model of the analyzed seeds was adopted in the form of a rotating ellipsoid whose major axis was seed length and minor axis was the average of seed thickness and width, calculated based on the following formula:

$$d = \frac{a + b}{2} \tag{1}$$

In the first stage of the analysis, a seed was placed on the surface of a string sieve with its longitudinal axis parallel to the strings, i.e. the string was supported by two adjacent strings (Fig. 2). In line with the principles of classical mechanics, it was assumed that the only external force acting upon the seed was the force of gravity G. In view of the sieve's angle of inclination, the force of gravity can be separated into two components: the force parallel to the strings G_y (which causes seeds to slide down the strings) and the force perpendicular to the strings G_z. Gravity force components can be expressed with the use of the below formula:

$$G_y = mg \sin\alpha \tag{2}$$

$$G_z = mg \cos\alpha \tag{3}$$

Component G_z can be decomposed into directions of the strings' normal ground reaction forces (Fig. 3):

$$G_{y1} = G_{y2} = \frac{G_z}{2\cos\varphi} = \frac{mg\cos\alpha}{2\cos\varphi} = N_1 = N_2 \tag{4}$$

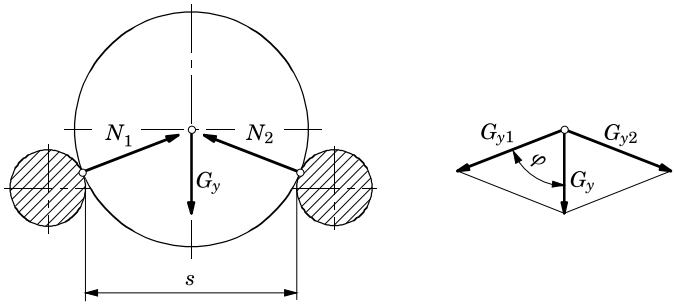

Fig. 3. Distribution of gravity force components and a normal ground reaction forces at a terminal point of the distance traveled by a seed on a string sieve

where angle φ is determined from a simple trigonometric function:

$$\sin\varphi = \frac{\frac{s}{2} + \frac{D_s}{2}}{\frac{d}{2} + \frac{D_s}{2}} = \frac{s + D_s}{d + D_s} \tag{5}$$

which is transformed to:

$$\varphi = \text{arc sin}\,\frac{s + D_s}{d + D_s} \tag{6}$$

When seeds are immobile, the friction force between a seed and a string can reach:

$$T_1 = \mu_s \cdot N_1 = \mu_s \cdot N_2 = T_2 \tag{7}$$

For a seed to slide down the strings, gravity force component G_y has to be greater than the net friction force:

$$G_y > 2T_1 \tag{8}$$

Equations (2), (4) and (7) were substituted into the above formula to produce:

$$mg\,\sin\alpha > 2 \cdot \mu_s \cdot \frac{mg\,\cos\alpha}{2\,\cos\varphi} \tag{9}$$

which was transformed to:

$$\tan\alpha > \frac{\mu_s}{\cos\varphi} \tag{10}$$

The above inequality was used to determine a sieve's critical angle of inclination which, when exceeded, will propel seeds into sliding motion:

$$\alpha = \text{arc tan}\,\frac{\mu_s}{\cos\varphi} \tag{11}$$

In accordance with formula (6), at given parameters of a string sieve, the critical angle of inclination will be determined only by the equivalent diameter of seed width and thickness.

When a sieve string is set at an angle that propels all seeds into motion, seeds will initially slide in uniformly accelerated motion. Angle φ will increase with an increase in the width of the separating groove, which increases normal force and friction force. Seed motion is inhibited (changed to uniformly retarded motion) as of the moment force component G_y becomes equal to friction:

$$mg \sin\alpha = \mu_k \cdot \frac{mg \cos\alpha}{\cos\varphi} \tag{12}$$

The angle between the direction of a normal force and the gravity force component at which the above forces are equalized can be determined by transforming formula (12) as follows:

$$\varphi = \text{arc cos} \frac{\mu_k}{\tan\alpha} \tag{13}$$

Angle φ is directly proportional to a seed's coefficient of sliding friction and inversely proportional to a string sieve's inclination angle.

As seeds continue to move down the sieve where the width of the separating grove gradually increases, their center of mass will be gradually lowered relative to the strings. The normal force of sieve strings will continue to increase, thus increasing friction. Those forces will not reach infinitely large values at the location where a seed passes through the screen because strings will deflect despite their initial pull tension. In view of the rapid increase in normal force at the final stage of seed motion along the screen, it was assumed that seeds should accelerate across minimum $^3/_4$ of the traveled distance and that their motion should be inhibited across maximum $^1/_4$ of the traveled distance to avoid mesh blockage. The above also applies to seeds characterized by the smallest equivalent diameter of width and thickness and the highest sliding friction coefficients which, in principle, ensures the continuity of the screening process. To fulfill the above condition, a string sieve's angle of inclination can be determined by transforming formula (12):

$$\alpha = \text{arc tan} \frac{\mu_k}{\cos\varphi} \tag{14}$$

Angle φ can be tied to the equivalent diameter of seed width and thickness based on the principle of similar triangles (KALINIEWICZ 2013a). In line with the above principle:

$$\frac{s_1 - s_p}{\frac{3}{4}e} = \frac{d - s_p}{e} \tag{15}$$

Formula (15) can be transformed to:

$$s_1 = \frac{3d + s_p}{4} \tag{16}$$

When the above formula is substituted into equation (6), the correlation with angle φ can be expressed as:

$$\varphi = \arcsin \frac{3d + s_p + 4D_s}{4(d + D_s)} \tag{17}$$

At given parameters of a string sieve, angle φ will be determined only by the equivalent diameter of seed width and thickness.

Materials and methods

The experimental material consisted of 120 seeds of every analyzed principal cereal species (wheat, rye, barley, oats and triticale). The physical parameters of the analyzed seeds have been described by KALINIEWICZ (2013b). For the needs of this experiment, only the results of seed thickness and seed width measurements and the coefficients of sliding and static friction of seeds are presented in Table 1. Seed thickness was determined with a special apparatus comprising a dial indicator, and seed width was measured under the MWM 2325 workshop microscope. Coefficients of sliding and static friction were determined with a special device for measuring the frictional properties of seeds.

Table 1

Statistical distribution of the physical parameters of seeds

Parameter	Cereal species				
	wheat $x \pm SD$	rye $x \pm SD$	barley $x \pm SD$	oats $x \pm SD$	triticale $x \pm SD$
a	2.87 ± 0.21	2.39 ± 0.25	2.87 ± 0.22	2.55 ± 0.15	2.70 ± 0.33
b	3.29 ± 0.31	2.65 ± 0.28	3.84 ± 0.30	3.15 ± 0.25	3.23 ± 0.38
μ_s	0.31 ± 0.03	0.30 ± 0.05	0.31 ± 0.03	0.35 ± 0.06	0.38 ± 0.06
μ_k	0.22 ± 0.03	0.19 ± 0.04	0.23 ± 0.03	0.16 ± 0.05	0.19 ± 0.06

Source: KALINIEWICZ (2013b).

The equivalent diameter of seed width and thickness was determined for each seed based on formula (1). The correlations between the equivalent diameter and the coefficients of sliding friction were analyzed. The range of variation in seed thickness and width was expanded by including the values determined for various cereal species by CHOSZCZ et al. (2010), GEODECKI and GRUNDAS (2003), GROCHOWICZ (1994), HEBDA and MICEK (2005, 2007), KALKAN and KARA (2011), KUSIŃSKA (2004), KUSIŃSKA et al. (2010), SADOWSKA and ŻABIŃSKI (2009), SEGIT et al. (2003) and SOLOGUBIK et al. (2013). The minimum and maximum values of the examined parameters were used to determine the range of variation in the equivalent diameter of seed thickness and width.

Calculations were performed for a string sieve variant equipped with steel strings where the width of the separating groove equaled s_p=1 mm at the beginning of the screen and s_k=5 mm at the end of the screen. String diameter was D_s=1 mm and string spacing was R_s=2 mm at the beginning of the screen (KALINIEWICZ 2013a).

Results and discussion

The analyzed seeds were arranged in the following descending order based on the average values of the equivalent diameter of seed width and thickness: barley, wheat, triticale, oats and rye (Tab. 2). The equivalent diameter was determined in the range of 1.79 mm (rye) to 3.81 (barley).

Table 2

Statistical distribution of the equivalent diameters of seed width and thickness

Cereal species	x_{min}	x_{max}	x	SD
Wheat	2.52	3.55	3.08	0.24
Rye	1.79	3.08	2.52	0.24
Barley	2.60	3.81	3.35	0.24
Oats	2.25	3.23	2.85	0.18
Triticale	1.99	3.57	2.97	0.34

KALINIEWICZ (2013b) demonstrated that physical dimensions (length, width, thickness), weight, volume, density and shape of cereal seeds do not significantly affect their frictional properties. Similar results were reported during attempts to determine correlations between the equivalent diameter of seed width and thickness and the seeds' coefficients of external friction (Tab. 3). Practically significant correlations, i.e. situations in which the coefficient of correlation exceeded 0.4, were not observed. A very weak correlation was noted only

between the equivalent diameter and the coefficient of static friction of barley seeds on a steel surface. In the remaining cases, correlation coefficients were below critical value. Every analyzed seed can be thus assigned a coefficient of sliding friction from the entire range of values determined for a given cereal species.

Table 3

Coefficients of linear correlation between the equivalent diameter of seed width and thickness and the coefficients of external friction of seeds

Cereal species	Coefficient of external friction	
	μ_s	μ_k
Wheat	-0.061	-0.048
Rye	-0.120	0.017
Barley	**-0.198**	-0.027
Oats	0.047	0.106
Triticale	-0.012	0.017

Bold font indicates that the correlation coefficient has exceeded critical value

HEBDA and MICEK (2005, 2007) demonstrated very strong correlations between physical dimensions of cereal grains. In line with the determined sign of the correlation coefficient, it was assumed that the observed correlations were directly proportional, e.g. low thickness corresponded to low width of cereal seeds. When the range of variability in physical dimensions was expanded, the equivalent diameter of seed width and thickness was determined in the range of 1.3 to 4.9 mm (Tab. 4). When the adopted parameters of a string sieve, i.e. $s=s_p=1$ mm and $d_s=1$ mm, were substituted into formula (6), the result was:

$$\varphi = \text{arc sin}\,\frac{2}{d+1} \tag{18}$$

Table 4

Equivalent diameters of seed width and thickness

Cereal species	d [mm]
Wheat	1.5–4.2
Rye	1.3–3.5
Barley	1.7–4.9
Oats	1.3–3.6
Triticale	1.8–4.2

The above equation and Figure 4 indicate that angle *o* decreases with an increase in the equivalent diameter of seed width and thickness. Subject to the seed's plumpness, angle φ can range from 19.8° (barley) to 60.4° (rye and wheat). The values of angle φ and the values of static friction coefficients were substituted into equation (11) to obtain a range of sieve angles at which seeds are propelled into motion (Fig. 5). The plumper the seeds, the smaller the angle of inclination. The following ranges of sieve angles were determined for the analyzed cereal species:

- wheat – 14.1–34.0°,
- rye – 14.5–40.1°,
- barley – 14.6–31.2°,
- oats – 14.2–44.0°,
- triticale – 16.0–38.1°.

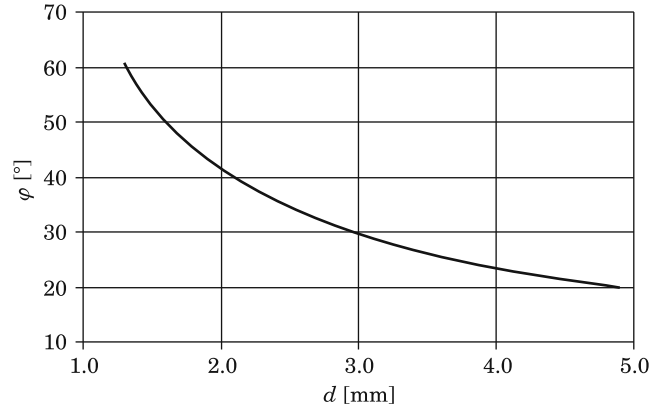

Fig. 4. Interrelation between the equivalent diameter of seed width and thickness and the angle of a string's normal ground reaction force relative to the gravity component (beginning of sieve)

The above indicates that seeds are propelled into motion when a string sieve is set at an estimated angle of 45°. The sieve's parameters were substituted into equation (17) to produce:

$$\varphi = \arcsin \frac{3d + 5}{4d + 4} \tag{19}$$

The values of angle φ were substituted into formula (14) to produce a range of sieve angles at which the ratio of the distance traveled by accelerating seeds and the distance traveled by slowing down seeds was 3:1. The above angle can assume the following range of values, subject to the equivalent diameter of seed width and thickness and the coefficient of sliding friction:

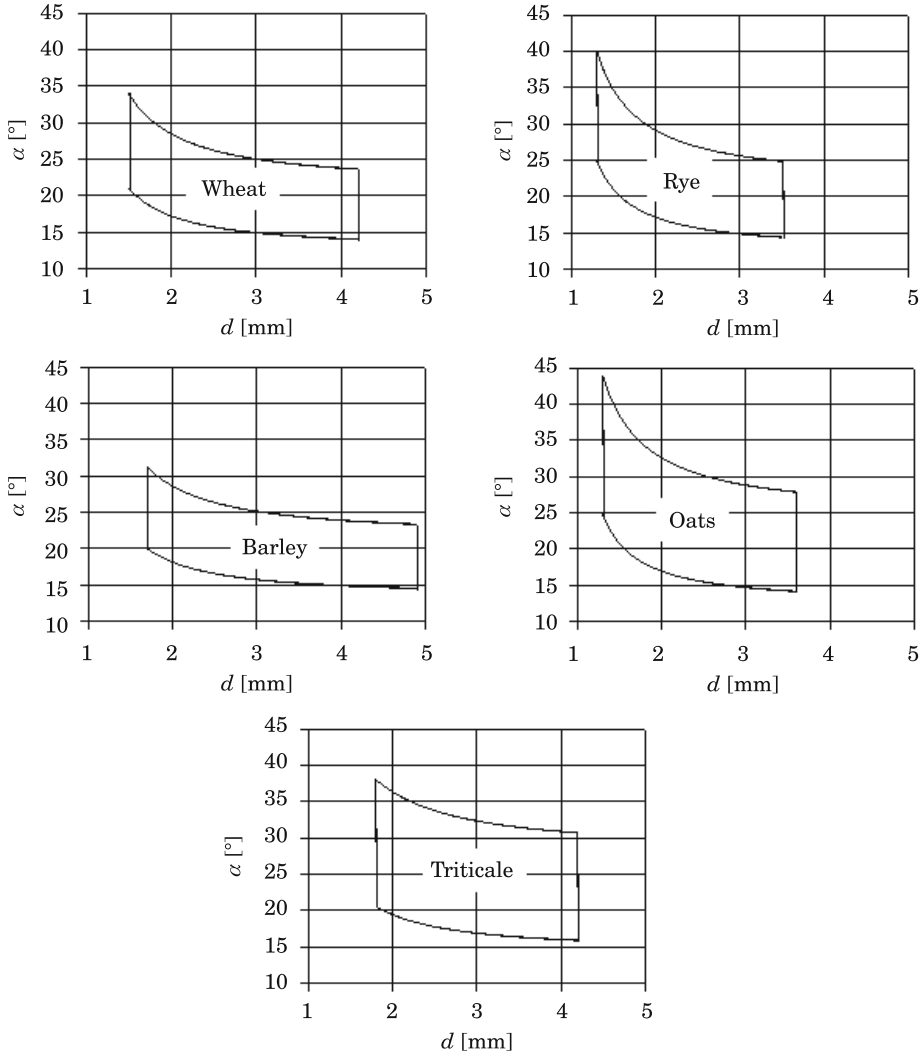

Fig. 5. Range of inclination angles of a string sieve at which cereal seeds are propelled into motion

– wheat – 13.9–41.9°,
– rye – 12.1–44.0°,
– barley – 12.4–39.9°,
– oats – 7.4–48.5°,
– triticale – 5.1–41.3°.

The range of variation is relatively broad, in particular for triticale seeds. Seed movement should satisfy the previously formulated conclusion to ensure the continuity of the separation process and to avoid mesh blockage. For this

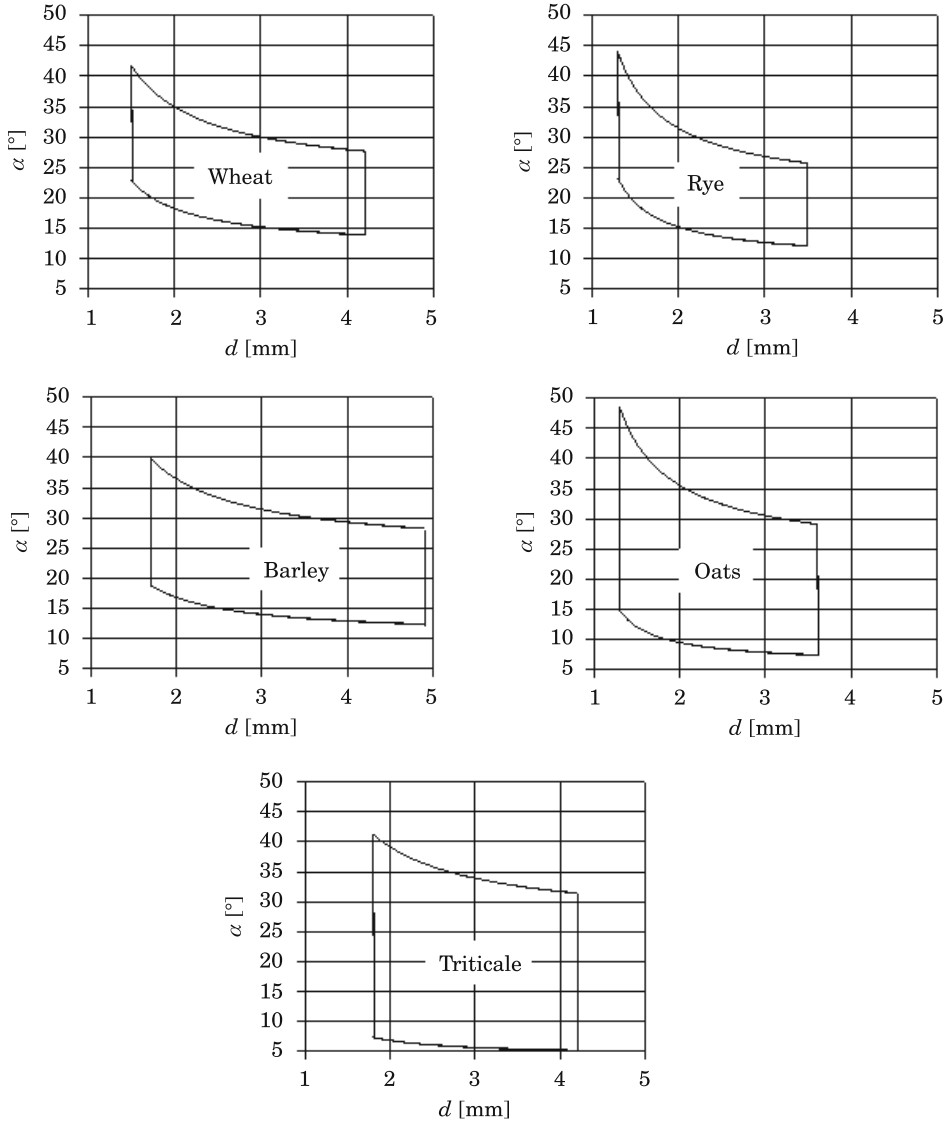

Fig. 6. Range of inclination angles of a string sieve which ensure the continuity of the separation process

reason, a string sieve should be set at the greatest angle. Oat seeds can be separated effectively at the angle of approximately 40°, whereas wheat, barley and triticale seeds require a greater angle of around 45°. To separate a mixture of the analyzed seed species, the inclination angle of a string sieve should be set at approximately 50°. According to GROCHOWICZ (1994), the angle of inclination

in modern separating devices rarely exceeds 8°. In this experiment, the choice of such a large inclination angle seems to be irrational, and it leads to an adverse increase in sieve height. In the discussed solution, the height of the sieve is increased by approximately 77% of its length to ensure the effective separation of all cereal seed species. To appropriately position a string sieve with the length of 1.2 m, its height has to be increased by 0.92 m. Large inclination angles are also undesirable because they prevent seed mixtures from being separated with the required precision. A mixture contains large seeds with relatively low coefficients of friction. Such seeds can attain high speeds, and they will fly over the location where they should theoretically pass through the screen. They will reach seed fractions characterized by significantly larger dimensions and higher coefficients of friction. To avoid the above scenario, the inclination angle of a string sieve should not exceed 10°, and seeds should be propelled into motion on the surface of the screen with the use of power brushes or by setting the entire separator bucket into motion.

Conclusions

1. In the presented solution which relies solely on the force of gravity, a string sieve has to be set at the angle of 50° to ensure the continuity of the separation process and avoid mesh blockage. At such a large angle, large seeds with a small coefficient of friction will attain excessive speeds, thus decreasing separation effectiveness.

2. The designed string sieve relies only on the force of gravity, and further research is needed to find more effective solutions. The effectiveness of the separation process can be enhanced by decreasing the inclination angle of the sieve to maximum 10° and propelling seeds into motion with the use of power brushes or by setting the entire separator bucket into reciprocating motion.

References

Berlage A.G., Cooper T.M., Carone R.A. 1984. *Seed sorting by machine vision*. Agricultural Engineering, 65(10): 14–17.

Căsăndroiu T., Popescu M., Voicu G. 2009. *A developing a mathematical model for simulating the seeds separation process on the plane sieves*. U.P.B. Sci. Bull., Series D, 71(3): 17–28.

Choszcz D., Konopka S., Zalewska K. 2010. *Characteristics of physical properties of selected varieties of spelt*. Inżynieria Rolnicza, 4(122): 23–28.

Gastón A.L., Abalone R.M., Giner S.A. 2002. *Wheat drying kinetics. Diffusivities for sphere and ellipsoid by finite elements*. J. Food Eng., 52, 313–332.

Geodecki M., Grundas S. 2003. *Characterization of geometrical features of single winter and spring wheat kernels*. Acta Agrophysica, 2(3): 531–538.

GROCHOWICZ J. 1994. *Maszyny do czyszczenia i sortowania nasion*. Wyd. Akademii Rolniczej, Lublin.
HEBDA T., MICEK P. 2005. *Dependences between geometrical features of cereal grain*. Inżynieria Rolnicza, 6: 233–241.
HEBDA T., MICEK P. 2007. *Geometric features of grain for selected corn varieties*. Inżynieria Rolnicza, 5(93): 187–193.
KALINIEWICZ Z. 2011. *Sito strunowe*. Zgłoszenie patentowe nr P.396745, 24.10.2011.
KALINIEWICZ Z. 2013a. *String sieve: design concept and parameters*. Technical Sciences, 16(2): 119–129.
KALINIEWICZ Z. 2013b. *Analysis of frictional properties of cereal seeds*. African Journal of Agricultural Research (in press).
KALKAN F., KARA M. 2011. *Handling, frictional and technological properties of wheat as affected by moisture content and cultivar*. Powder Technology, 213: 116–122.
KUSIŃSKA E. 2004. *The influence of storage time, moisture kontent and self-warming up on selected geometrical parameters of oat grain*. MOTROL – Motoryzacja i Energetyka Rolnictwa, 6: 146–153.
KUSIŃSKA E., KOBUS Z., NADULSKI R. 2010. *Impact of humidity on physical and geometrical properties of Slavic varieties of rye grains*. Inżynieria Rolnicza, 4(122): 151–156.
LI J., WEBB C., PANDIELLA S.S., CAMPBELL G.M. 2002. *Numerical simulation of separation of crop seeds by screening – effect of particle bed depth*. Trans IChemE, 80(C): 109–117.
RAWA T. 1992. *A study of the buckwheat grain clearing effectiveness*. Acta Acad. Agricult. Techn. Ols., Aedif. Mech., 22, Supplementum A.
RAWA T., WIERZBICKI K., PIETKIEWICZ T. 1990. *Potential effectiveness of rape seeds cleaning according to geometrical characteristics*. Acta Acad. Agricult. Tech. Olst. Aedif. Mech., 20: 117–129.
SADOWSKA U., ŻABIŃSKI A. 2009. *Selected physical properties for seeds of gymnosperm barley grown in a mixture with edible lentil*. Inżynieria Rolnicza, 6(115): 229–236.
SEGIT Z., SZWED G., SZWED-URBAŚ K. 2003. *Damage to durum wheat grains as a result of dynamic loading*. Acta Agrophysica, 2(4): 841–849.
SIMONYAN K.J., YILJEP Y.D. 2008. *Investigating Grain Separation and Cleaning Efficiency Distribution of a Conventional Stationary Rasp-bar Sorghum Thresher*. Agricultural Engineering International: the CIGR Ejournal Manuscript PM 07 028, X: 1–13.
SOLOGUBIK C.A., CAMPAÑONE L.A., PAGANO A.M., GELY M.C. 2013. *Effect of moisture content on some physical properties of barley*. Industrial Crops and Products, 43: 762–767.
VOICU G., CĂSĂNDROIU T. 2009. *Comparative analysis of mathematical models used in account of separation process of the seeds on the cleaning sieves system from cereals combines*. Machinery Building, 11–12: 37–39.
WANG Y.S., CHUNG D.S., SPILLMAN C.K., ECKHOFF S.R., RHEE C., CONVERSE H.H. 1994. *Evaluation of Laboratory Grain Cleaning and Separating Equipment, Part I. American Society of Agricultural Engineers*. Transactions of ASAE, 37(2): 507–513.
WIERZBICKI K., PIETKIEWICZ T., CHOSZCZ D., MAŃKOWSKI S. 1991. *Effectiveness of the wheat grain cleaning process with complex movement of sieve basket*. Acta Acad. Agricult. Techn. Ols., Aedif. Mech., 22: 179–189.
ZDYBEL A., GAWŁOWSKI S., LASKOWSKI J. 2009. *Influence of moisture content on some physical properties of rye grains*. Acta Agrophysica, 14(1): 243–255.
ŻABIŃSKI A., SADOWSKA U. 2010. *Selected physical properties of the spelt grain*. Inżynieria Rolnicza, 4(122): 309–317.